nature

Accelerated Article Preview

DOCK2 is involved in the host genetics and biology of severe COVID-19

Received: 26 October 2021

Accepted: 28 July 2022

Accelerated Article Preview

Cite this article as: Namkoong, H. et al. DOCK2 is involved in the host genetics and biology of severe COVID-19. *Nature* https://doi.org/10.1038/s41586-022-05163-5 (2022)

Ho Namkoong, Ryuya Edahiro, Tomomi Takano, Hiroshi Nishihara, Yuya Shirai, Kyuto Sonehara, Hiromu Tanaka, Shuhei Azekawa, Yohei Mikami, Ho Lee, Takanori Hasegawa, Koji Okudela, Daisuke Okuzaki, Daisuke Motooka, Masahiro Kanai, Tatsuhiko Naito, Kenichi Yamamoto, Qingbo S. Wang, Ryunosuke Saiki, Rino Ishihara, Yuta Matsubara, Junko Hamamoto, Hiroyuki Hayashi, Yukihiro Yoshimura, Natsuo Tachikawa, Emmy Yanagita, Takayoshi Hyugaji, Eigo Shimizu, Kotoe Katayama, Yasuhiro Kato, Takayoshi Morita, Kazuhisa Takahashi, Norihiro Harada, Toshio Naito, Makoto Hiki, Yasushi Matsushita, Haruhi Takagi, Ryousuke Aoki, Ai Nakamura, Sonoko Harada, Hitoshi Sasano, Hiroki Kabata, Katsunori Masaki, Hirofumi Kamata, Shinnosuke Ikemura, Shotaro Chubachi, Satoshi Okamori, Hideki Terai, Atsuho Morita, Takanori Asakura, Junichi Sasaki, Hiroshi Morisaki, Yoshifumi Uwamino, Kosaku Nanki, Sho Uchida, Shunsuke Uno, Tomoyasu Nishimura, Takashi Ishiguro, Taisuke Isono, Shun Shibata, Yuma Matsui, Chiaki Hosoda, Kenji Takano, Takashi Nishida, Yoichi Kobayashi, Yotaro Takaku, Noboru Takayanagi, Soichiro Ueda, Ai Tada, Masayoshi Miyawaki, Masaomi Yamamoto, Eriko Yoshida, Reina Hayashi, Tomoki Nagasaka, Sawako Arai, Yutaro Kaneko, Kana Sasaki, Etsuko Tagaya, Masatoshi Kawana, Ken Arimura, Kunihiko Takahashi, Tatsuhiko Anzai, Satoshi Ito, Akifumi Endo, Yuji Uchimura, Yasunari Miyazaki, Takayuki Honda, Tomoya Tateishi, Shuji Tohda, Naoya Ichimura, Kazunari Sonobe, Chihiro Tani Sassa, Jun Nakajima, Yasushi Nakano, Yukiko Nakajima, Ryusuke Anan, Ryosuke Arai, Yuko Kurihara, Yuko Harada, Kazumi Nishio, Tetsuya Ueda, Masanori Azuma, Ryuichi Saito, Toshikatsu Sado, Yoshimune Miyazaki, Ryuichi Sato, Yuki Haruta, Tadao Nagasaki, Yoshinori Yasui, Yoshinori Hasegawa, Yoshikazu Mutoh, Tomoki Kimura, Tomonori Sato, Reoto Takei, Satoshi Hagimoto, Yoichiro Noguchi, Yasuhiko Yamano, Hajime Sasano, Sho Ota, Yasushi Nakamori, Kazuhisa Yoshiya, Fukuki Saito, Tomoyuki Yoshihara, Daiki Wada, Hiromu Iwamura, Syuji Kanayama, Shuhei Maruyama, Takashi Yoshiyama, Ken Ohta, Hiroyuki Kokuto, Hideo Ogata, Yoshiaki Tanaka, Kenichi Arakawa, Masafumi Shimoda, Takeshi Osawa, Hiroki Tateno, Isano Hase, Shuichi Yoshida, Shoji Suzuki, Miki Kawada, Hirohisa Horinouchi, Fumitake Saito, Keiko Mitamura, Masao Hagihara, Junichi Ochi, Tomoyuki Uchida, Rie Baba, Daisuke Arai, Takayuki Ogura, Hidenori Takahashi, Shigehiro Hagiwara, Genta Nagao, Shunichiro Konishi, Ichiro Nakachi, Koji Murakami, Mitsuhiro Yamada, Hisatoshi Sugiura, Hirohito Sano, Shuichiro Matsumoto, Nozomu Kimura, Yoshinao Ono, Hiroaki Baba, Yusuke Suzuki, Sohei Nakayama, Keita Masuzawa, Shinichi Namba, Ken Suzuki, Yoko Naito, Yu-Chen Liu, Ayako Takuwa, Fuminori Sugihara, James B. Wing, Shuhei Sakakibara, Nobuyuki Hizawa, Takayuki Shiroyama, Satoru Miyawaki, Yusuke Kawamura, Akiyoshi Nakayama, Hirotaka Matsuo, Yuichi Maeda, Takuro Nii, Yoshimi Noda, Takayuki Niitsu, Yuichi Adachi, Takatoshi Enomoto, Saori Amiya, Reina Hara, Yuta Yamaguchi, Teruaki Murakami, Tomoki Kuge, Kinnosuke Matsumoto, Yuji Yamamoto, Makoto Yamamoto, Midori Yoneda, Toshihiro Kishikawa, Shuhei Yamada, Shuhei Kawabata, Noriyuki Kijima, Masatoshi Takagaki, Noah Sasa, Yuya Ueno, Motoyuki Suzuki, Norihiko Takemoto, Hirotaka Eguchi, Takahito Fukusumi, Takao Imai, Munehisa Fukushima, Haruhiko Kishima, Hidenori Inohara, Kazunori Tomono, Kazuto Kato, Meiko Takahashi, Fumihiko Matsuda, Haruhiko Hirata, Yoshito Takeda, Hidefumi Koh, Tadashi Manabe, Yohei Funatsu, Fumimaro Ito, Takahiro Fukui, Keisuke Shinozuka, Sumiko Kohashi, Masatoshi Miyazaki, Tomohisa Shoko, Mitsuaki Kojima, Tomohiro Adachi, Motonao Ishikawa, Kenichiro Takahashi, Takashi Inoue, Toshiyuki Hirano, Keigo Kobayashi, Hatsuyo Takaoka, Kazuyoshi Watanabe, Naoki Miyazawa, Yasuhiro Kimura, Reiko Sado, Hideyasu Sugimoto, Akane Kamiya, Naota Kuwahara, Akiko Fujiwara, Tomohiro Matsunaga, Yoko Sato, Takenori Okada, Yoshihiro Hirai, Hidetoshi Kawashima, Atsuya Narita, Kazuki Niwa, Yoshiyuki Sekikawa, Koichi Nishi, Masaru Nishitsuji, Mayuko Tani, Junya Suzuki, Hiroki Nakatsumi, Takashi Ogura, Hideya Kitamura, Eri Hagiwara, Kota Murohashi, Hiroko Okabayashi, Takao Mochimaru, Shigenari Nukaga, Ryosuke Satomi,

ACCELERATED ARTICLE PREVIEW

Yoshitaka Oyamada, Nobuaki Mori, Tomoya Baba, Yasutaka Fukui, Mitsuru Odate, Shuko Mashimo, Yasushi Makino, Kazuma Yagi, Mizuha Hashiguchi, Junko Kagyo, Tetsuya Shiomi, Satoshi Fuke, Hiroshi Saito, Tomoya Tsuchida, Shigeki Fujitani, Mumon Takita, Daiki Morikawa, Toru Yoshida, Takehiro Izumo, Minoru Inomata, Naoyuki Kuse, Nobuyasu Awano, Mari Tone, Akihiro Ito, Yoshihiko Nakamura, Kota Hoshino, Junichi Maruyama, Hiroyasu Ishikura, Tohru Takata, Toshio Odani, Masaru Amishima, Takeshi Hattori, Yasuo Shichinohe, Takashi Kagaya, Toshiyuki Kita, Kazuhide Ohta, Satoru Sakagami, Kiyoshi Koshida, Kentaro Hayashi, Tetsuo Shimizu, Yutaka Kozu, Hisato Hiranuma, Yasuhiro Gon, Namiki Izumi, Kaoru Nagata, Ken Ueda, Reiko Taki, Satoko Hanada, Kodai Kawamura, Kazuya Ichikado, Kenta Nishiyama, Hiroyuki Muranaka, Kazunori Nakamura, Naozumi Hashimoto, Keiko Wakahara, Sakamoto Koji, Norihito Omote, Akira Ando, Nobuhiro Kodama, Yasunari Kaneyama, Shunsuke Maeda, Takashige Kuraki, Takemasa Matsumoto, Koutaro Yokote, Taka-Aki Nakada, Ryuzo Abe, Taku Oshima, Tadanaga Shimada, Masahiro Harada, Takeshi Takahashi, Hiroshi Ono, Toshihiro Sakurai, Takayuki Shibusawa, Yoshifumi Kimizuka, Akihiko Kawana, Tomoya Sano, Chie Watanabe, Ryohei Suematsu, Hisako Sageshima, Ayumi Yoshifuji, Kazuto Ito, Saeko Takahashi, Kota Ishioka, Morio Nakamura, Makoto Masuda, Aya Wakabayashi, Hiroki Watanabe, Suguru Ueda, Masanori Nishikawa, Yusuke Chihara, Mayumi Takeuchi, Keisuke Onoi, Jun Shinozuka, Atsushi Sueyoshi, Yoji Nagasaki, Masaki Okamoto, Sayoko Ishihara, Masatoshi Shimo, Yoshihisa Tokunaga, Yu Kusaka, Takehiko Ohba, Susumu Isogai, Aki Ogawa, Takuya Inoue, Satoru Fukuyama, Yoshihiro Eriguchi, Akiko Yonekawa, Keiko Kan-o, Koichiro Matsumoto, Kensuke Kanaoka, Shoichi Ihara, Kiyoshi Komuta, Yoshiaki Inoue, Shigeru Chiba, Kunihiro Yamagata, Yuji Hiramatsu, Hirayasu Kai, Koichiro Asano, Tsuyoshi Oguma, Yoko Ito, Satoru Hashimoto, Masaki Yamasaki, Yu Kasamatsu, Yuko Komase, Naoya Hida, Takahiro Tsuburai, Baku Oyama, Minoru Takada, Hidenori Kanda, Yuichiro Kitagawa, Tetsuya Fukuta, Takahito Miyake, Shozo Yoshida, Shinji Ogura, Shinji Abe, Yuta Kono, Yuki Togashi, Hiroyuki Takoi, Ryota Kikuchi, Shinichi Ogawa, Tomouki Ogata, Shoichiro Ishihara, Arihiko Kanehiro, Shinji Ozaki, Yasuko Fuchimoto, Sae Wada, Nobukazu Fujimoto, Kei Nishiyama, Mariko Terashima, Satoru Beppu, Kosuke Yoshida, Osamu Narumoto, Hideaki Nagai, Nobuharu Ooshima, Mitsuru Motegi, Akira Umeda, Kazuya Miyagawa, Hisato Shimada, Mayu Endo, Yoshiyuki Ohira, Masafumi Watanabe, Sumito Inoue, Akira Igarashi, Masamichi Sato, Hironori Sagara, Akihiko Tanaka, Shin Ohta, Tomoyuki Kimura, Yoko Shibata, Yoshinori Tanino, Takefumi Nikaido, Hiroyuki Minemura, Yuki Sato, Yuichiro Yamada, Takuya Hashino, Masato Shinoki, Hajime Iwagoe, Hiroshi Takahashi, Kazuhiko Fujii, Hiroto Kishi, Masayuki Kanai, Tomonori Imamura, Tatsuya Yamashita, Masakiyo Yatomi, Toshitaka Maeno, Shinichi Hayashi, Mai Takahashi, Mizuki Kuramochi, Isamu Kamimaki, Yoshiteru Tominaga, Tomoo Ishii, Mitsuyoshi Utsugi, Akihiro Ono, Toru Tanaka, Takeru Kashiwada, Kazue Fujita, Yoshinobu Saito, Masahiro Seike, Hiroko Watanabe, Hiroto Matsuse, Norio Kodaka, Chihiro Nakano, Takeshi Oshio, Takatomo Hirouchi, Shohei Makino, Moritoki Egi, The Biobank Japan Project, Yosuke Omae, Yasuhito Nannya, Takafumi Ueno, Kazuhiko Katayama, Masumi Ai, Yoshinori Fukui, Atsushi Kumanogoh, Toshiro Sato, Naoki Hasegawa, Katsushi Tokunaga, Makoto Ishii, Ryuji Koike, Yuko Kitagawa, Akinori Kimura, Seiya Imoto, Satoru Miyano, Seishi Ogawa, Takanori Kanai, Koichi Fukunaga & Yukinori Okada

This is a PDF file of a peer-reviewed paper that has been accepted for publication. Although unedited, the content has been subjected to preliminary formatting. Nature is providing this early version of the typeset paper as a service to our authors and readers. The text and figures will undergo copyediting and a proof review before the paper is published in its final form. Please note that during the production process errors may be discovered which could affect the content, and all legal disclaimers apply.

ACCELERATED ARTICLE PREVIEW

DOCK2 is involved in the host genetics and biology of severe COVID-19

Ho Namkoong[1,195], Ryuya Edahiro[2,3,195], Tomomi Takano[4], Hiroshi Nishihara[5], Yuya Shirai[2,3], Kyuto Sonehara[2,6], Hiromu Tanaka[7], Shuhei Azekawa[7], Yohei Mikami[8], Ho Lee[7], Takanori Hasegawa[9], Koji Okudela[10], Daisuke Okuzaki[11], Daisuke Motooka[12], Masahiro Kanai[13], Tatsuhiko Naito[2], Kenichi Yamamoto[2], Qingbo S Wang[2], Ryunosuke Saiki[14], Rino Ishihara[8], Yuta Matsubara[8], Junko Hamamoto[7], Hiroyuki Hayashi[15], Yukihiro Yoshimura[16], Natsuo Tachikawa[16], Emmy Yanagita[5], Takayoshi Hyugaji[17], Eigo Shimizu[17], Kotoe Katayama[17], Yasuhiro Kato[3,18], Takayoshi Morita[3,18], Kazuhisa Takahashi[19], Norihiro Harada[19], Toshio Naito[20], Makoto Hiki[21,22], Yasushi Matsushita[23], Haruhi Takagi[19], Ryousuke Aoki[24], Ai Nakamura[19], Sonoko Harada[19,25], Hitoshi Sasano[19], Hiroki Kabata[7], Katsunori Masaki[7], Hirofumi Kamata[7], Shinnosuke Ikemura[7], Shotaro Chubachi[7], Satoshi Okamori[7], Hideki Terai[7], Atsuho Morita[7], Takanori Asakura[7], Junichi Sasaki[26], Hiroshi Morisaki[27], Yoshifumi Uwamino[28], Kosaku Nanki[8], Sho Uchida[1], Shunsuke Uno[1], Tomoyasu Nishimura[29,1], Takashi Ishiguro[30], Taisuke Isono[30], Shun Shibata[30], Yuma Matsui[30], Chiaki Hosoda[30], Kenji Takano[30], Takashi Nishida[30], Yoichi Kobayashi[30], Yotaro Takaku[30], Noboru Takayanagi[30], Soichiro Ueda[31], Ai Tada[31], Masayoshi Miyawaki[31], Masaomi Yamamoto[31], Eriko Yoshida[31], Reina Hayashi[31], Tomoki Nagasaka[31], Sawako Arai[31], Yutaro Kaneko[31], Kana Sasaki[31], Etsuko Tagaya[32], Masatoshi Kawana[33], Ken Arimura[32], Kunihiko Takahashi[9], Tatsuhiko Anzai[9], Satoshi Ito[9], Akifumi Endo[34], Yuji Uchimura[35], Yasunari Miyazaki[36], Takayuki Honda[36], Tomoya Tateishi[36], Shuji Tohda[37], Naoya Ichimura[37], Kazunari Sonobe[37], Chihiro Tani Sassa[37], Jun Nakajima[37], Yasushi Nakano[38], Yukiko Nakajima[38], Ryusuke Anan[38], Ryosuke Arai[38], Yuko Kurihara[38], Yuko Harada[38], Kazumi Nishio[38], Tetsuya Ueda[39], Masanori Azuma[39], Ryuichi Saito[39], Toshikatsu Sado[39], Yoshimune Miyazaki[39], Ryuichi Sato[39], Yuki Haruta[39], Tadao Nagasaki[39], Yoshinori Yasui[40], Yoshinori Hasegawa[39], Yoshikazu Mutoh[41], Tomoki Kimura[42], Tomonori Sato[42], Reoto Takei[42], Satoshi Hagimoto[42], Yoichiro Noguchi[42], Yasuhiko Yamano[42], Hajime Sasano[42], Sho Ota[42], Yasushi Nakamori[43], Kazuhisa Yoshiya[43], Fukuki Saito[43], Tomoyuki Yoshihara[43], Daiki Wada[43], Hiromu Iwamura[43], Syuji Kanayama[43], Shuhei Maruyama[43], Takashi Yoshiyama[44], Ken Ohta[44], Hiroyuki Kokuto[44], Hideo Ogata[44], Yoshiaki Tanaka[44], Kenichi Arakawa[44], Masafumi Shimoda[44], Takeshi Osawa[44], Hiroki Tateno[45], Isano Hase[45], Shuichi Yoshida[45], Shoji Suzuki[45], Miki Kawada[46], Hirohisa Horinouchi[47], Fumitake Saito[48], Keiko Mitamura[49], Masao Hagihara[50], Junichi Ochi[48], Tomoyuki Uchida[50], Rie Baba[51], Daisuke Arai[51], Takayuki Ogura[51], Hidenori Takahashi[51], Shigehiro Hagiwara[51], Genta Nagao[51], Shunichiro Konishi[51], Ichiro Nakachi[51], Koji Murakami[52], Mitsuhiro Yamada[52], Hisatoshi Sugiura[52], Hirohito Sano[52], Shuichiro Matsumoto[52], Nozomu Kimura[52], Yoshinao Ono[52], Hiroaki Baba[53], Yusuke Suzuki[54], Sohei Nakayama[54], Keita Masuzawa[54], Shinichi Namba[2], Ken Suzuki[2], Yoko Naito[12], Yu-Chen Liu[11], Ayako Takuwa[11], Fuminori Sugihara[55], James B Wing[56,57], Shuhei Sakakibara[58], Nobuyuki Hizawa[59], Takayuki Shiroyama[3], Satoru Miyawaki[60], Yusuke Kawamura[61], Akiyoshi Nakayama[61], Hirotaka Matsuo[61], Yuichi Maeda[3], Takuro Nii[3], Yoshimi Noda[3], Takayuki Niitsu[3], Yuichi Adachi[3], Takatoshi Enomoto[3], Saori Amiya[3], Reina Hara[3], Yuta Yamaguchi[3,18], Teruaki Murakami[3,18], Tomoki Kuge[3], Kinnosuke Matsumoto[3], Yuji Yamamoto[3], Makoto Yamamoto[3], Midori Yoneda[3], Toshihiro Kishikawa[2,62,63], Shuhei Yamada[64], Shuhei Kawabata[64], Noriyuki Kijima[64], Masatoshi Takagaki[64], Noah Sasa[2,62], Yuya Ueno[62], Motoyuki Suzuki[62], Norihiko Takemoto[62], Hirotaka Eguchi[62], Takahito Fukusumi[62], Takao Imai[62], Munehisa Fukushima[62,65], Haruhiko Kishima[64], Hidenori Inohara[62], Kazunori Tomono[66], Kazuto Kato[67], Meiko Takahashi[68], Fumihiko Matsuda[68], Haruhiko Hirata[3], Yoshito Takeda[3], Hidefumi Koh[69], Tadashi Manabe[69], Yohei Funatsu[69], Fumimaro Ito[69], Takahiro Fukui[69], Keisuke Shinozuka[69], Sumiko Kohashi[69],

ACCELERATED ARTICLE PREVIEW

Masatoshi Miyazaki[69], Tomohisa Shoko[70], Mitsuaki Kojima[70], Tomohiro Adachi[70], Motonao Ishikawa[71], Kenichiro Takahashi[72], Takashi Inoue[73], Toshiyuki Hirano[73], Keigo Kobayashi[73], Hatsuyo Takaoka[73], Kazuyoshi Watanabe[74], Naoki Miyazawa[75], Yasuhiro Kimura[75], Reiko Sado[75], Hideyasu Sugimoto[75], Akane Kamiya[76], Naota Kuwahara[77], Akiko Fujiwara[77], Tomohiro Matsunaga[77], Yoko Sato[77], Takenori Okada[77], Yoshihiro Hirai[78], Hidetoshi Kawashima[78], Atsuya Narita[78], Kazuki Niwa[79], Yoshiyuki Sekikawa[79], Koichi Nishi[80], Masaru Nishitsuji[80], Mayuko Tani[80], Junya Suzuki[80], Hiroki Nakatsumi[80], Takashi Ogura[81], Hideya Kitamura[81], Eri Hagiwara[81], Kota Murohashi[81], Hiroko Okabayashi[81], Takao Mochimaru[82,83], Shigenari Nukaga[82], Ryosuke Satomi[82], Yoshitaka Oyamada[82,83], Nobuaki Mori[84], Tomoya Baba[85], Yasutaka Fukui[85], Mitsuru Odate[85], Shuko Mashimo[85], Yasushi Makino[85], Kazuma Yagi[86], Mizuha Hashiguchi[86], Junko Kagyo[86], Tetsuya Shiomi[86], Satoshi Fuke[87], Hiroshi Saito[87], Tomoya Tsuchida[88], Shigeki Fujitani[89], Mumon Takita[89], Daiki Morikawa[89], Toru Yoshida[89], Takehiro Izumo[90], Minoru Inomata[90], Naoyuki Kuse[90], Nobuyasu Awano[90], Mari Tone[90], Akihiro Ito[91], Yoshihiko Nakamura[92], Kota Hoshino[92], Junichi Maruyama[92], Hiroyasu Ishikura[92], Tohru Takata[93], Toshio Odani[94], Masaru Amishima[95], Takeshi Hattori[95], Yasuo Shichinohe[96], Takashi Kagaya[97], Toshiyuki Kita[97], Kazuhide Ohta[97], Satoru Sakagami[97], Kiyoshi Koshida[97], Kentaro Hayashi[98], Tetsuo Shimizu[98], Yutaka Kozu[98], Hisato Hiranuma[98], Yasuhiro Gon[98], Namiki Izumi[99], Kaoru Nagata[99], Ken Ueda[99], Reiko Taki[99], Satoko Hanada[99], Kodai Kawamura[100], Kazuya Ichikado[100], Kenta Nishiyama[100], Hiroyuki Muranaka[100], Kazunori Nakamura[100], Naozumi Hashimoto[101], Keiko Wakahara[101], Sakamoto Koji[101], Norihito Omote[101], Akira Ando[101], Nobuhiro Kodama[102], Yasunari Kaneyama[102], Shunsuke Maeda[102], Takashige Kuraki[103], Takemasa Matsumoto[103], Koutaro Yokote[104], Taka-Aki Nakada[105], Ryuzo Abe[105], Taku Oshima[105], Tadanaga Shimada[105], Masahiro Harada[106], Takeshi Takahashi[106], Hiroshi Ono[106], Toshihiro Sakurai[106], Takayuki Shibusawa[106], Yoshifumi Kimizuka[107], Akihiko Kawana[107], Tomoya Sano[107], Chie Watanabe[107], Ryohei Suematsu[107], Hisako Sageshima[108], Ayumi Yoshifuji[109], Kazuto Ito[109], Saeko Takahashi[110], Kota Ishioka[110], Morio Nakamura[110], Makoto Masuda[111], Aya Wakabayashi[111], Hiroki Watanabe[111], Suguru Ueda[111], Masanori Nishikawa[111], Yusuke Chihara[112], Mayumi Takeuchi[112], Keisuke Onoi[112], Jun Shinozuka[112], Atsushi Sueyoshi[112], Yoji Nagasaki[113], Masaki Okamoto[114,115], Sayoko Ishihara[116], Masatoshi Shimo[116], Yoshihisa Tokunaga[114,115], Yu Kusaka[117], Takehiko Ohba[117], Susumu Isogai[117], Aki Ogawa[117], Takuya Inoue[117], Satoru Fukuyama[118], Yoshihiro Eriguchi[119], Akiko Yonekawa[119], Keiko Kan-o[118], Koichiro Matsumoto[118], Kensuke Kanaoka[120], Shoichi Ihara[120], Kiyoshi Komuta[120], Yoshiaki Inoue[121], Shigeru Chiba[122], Kunihiro Yamagata[123], Yuji Hiramatsu[124], Hirayasu Kai[123], Koichiro Asano[125], Tsuyoshi Oguma[125], Yoko Ito[125], Satoru Hashimoto[126], Masaki Yamasaki[126], Yu Kasamatsu[127], Yuko Komase[128], Naoya Hida[128], Takahiro Tsuburai[128], Baku Oyama[128], Minoru Takada[129], Hidenori Kanda[129], Yuichiro Kitagawa[130], Tetsuya Fukuta[130], Takahito Miyake[130], Shozo Yoshida[130], Shinji Ogura[130], Shinji Abe[131], Yuta Kono[131], Yuki Togashi[131], Hiroyuki Takoi[131], Ryota Kikuchi[131], Shinichi Ogawa[132], Tomouki Ogata[132], Shoichiro Ishihara[132], Arihiko Kanehiro[133,134], Shinji Ozaki[133], Yasuko Fuchimoto[133], Sae Wada[133], Nobukazu Fujimoto[133], Kei Nishiyama[135], Mariko Terashima[136], Satoru Beppu[136], Kosuke Yoshida[136], Osamu Narumoto[137], Hideaki Nagai[137], Nobuharu Ooshima[137], Mitsuru Motegi[138], Akira Umeda[139], Kazuya Miyagawa[140], Hisato Shimada[141], Mayu Endo[142], Yoshiyuki Ohira[139], Masafumi Watanabe[143], Sumito Inoue[143], Akira Igarashi[143], Masamichi Sato[143], Hironori Sagara[144], Akihiko Tanaka[144], Shin Ohta[144], Tomoyuki Kimura[144], Yoko Shibata[145], Yoshinori Tanino[145], Takefumi Nikaido[145], Hiroyuki Minemura[145], Yuki Sato[145], Yuichiro Yamada[146], Takuya Hashino[146], Masato Shinoki[146], Hajime Iwagoe[147], Hiroshi Takahashi[148], Kazuhiko Fujii[148], Hiroto Kishi[148], Masayuki Kanai[149], Tomonori Imamura[149], Tatsuya Yamashita[149], Masakiyo Yatomi[150], Toshitaka Maeno[150], Shinichi Hayashi[151], Mai Takahashi[151], Mizuki Kuramochi[151], Isamu Kamimaki[151], Yoshiteru Tominaga[151], Tomoo Ishii[152], Mitsuyoshi

ACCELERATED ARTICLE PREVIEW

Utsugi[153], Akihiro Ono[153], Toru Tanaka[154], Takeru Kashiwada[154], Kazue Fujita[154], Yoshinobu Saito[154], Masahiro Seike[154], Hiroko Watanabe[155], Hiroto Matsuse[156], Norio Kodaka[156], Chihiro Nakano[156], Takeshi Oshio[156], Takatomo Hirouchi[156], Shohei Makino[157], Moritoki Egi[157], The Biobank Japan Project*, Yosuke Omae[158], Yasuhito Nannya[14], Takafumi Ueno[159], Kazuhiko Katayama[160], Masumi Ai[161], Yoshinori Fukui[162], Atsushi Kumanogoh[3,18,6,57], Toshiro Sato[163], Naoki Hasegawa[1], Katsushi Tokunaga[158], Makoto Ishii[7], Ryuji Koike[164], Yuko Kitagawa[165], Akinori Kimura[166], Seiya Imoto[17], Satoru Miyano[9,196], Seishi Ogawa[14,167,168,196], Takanori Kanai[8,169,196], Koichi Fukunaga[7,196], Yukinori Okada[2,6,57,170-172,196]

1. Department of Infectious Diseases, Keio University School of Medicine, Tokyo, Japan.
2. Department of Statistical Genetics, Osaka University Graduate School of Medicine, Suita, Japan.
3. Department of Respiratory Medicine and Clinical Immunology, Osaka University Graduate School of Medicine, Suita, Japan.
4. Laboratory of Veterinary Infectious Disease, School of Veterinary Medicine, Kitasato University, Aomori, Japan.
5. Genomics Unit, Keio Cancer Center, Keio University Hospital, Tokyo, Japan.
6. Integrated Frontier Research for Medical Science Division, Institute for Open and Transdisciplinary Research Initiatives, Osaka University, Suita, Japan.
7. Division of Pulmonary Medicine, Department of Medicine, Keio University School of Medicine, Tokyo, Japan
8. Division of Gastroenterology and Hepatology, Department of Medicine, Keio University School of Medicine, Tokyo, Japan.
9. M&D Data Science Center, Tokyo Medical and Dental University, Tokyo, Japan.
10. Department of Pathology, Graduate School of Medicine, Yokohama City University, Yokohama, Japan.
11. Single Cell Genomics, Human Immunology, WPI Immunology Frontier Research Center, Osaka University, Suita, Japan.
12. Genome Information Research Center, Research Institute for Microbial Diseases, Osaka University, Suita, Japan.
13. Department of Biomedical Informatics, Harvard Medical School, Boston, MA, USA
14. Department of Pathology and Tumor Biology, Kyoto University, Kyoto, Japan.
15. Division of Pathology, Yokohama Municipal Citizen's Hospital, Yokohama, Japan.
16. Division of Infectious Disease, Yokohama Municipal Citizen's Hospital, Yokohama, Japan.
17. Division of Health Medical Intelligence, Human Genome Center, the Institute of Medical Science, the University of Tokyo, Tokyo, Japan.
18. Department of Immunopathology, Immunology Frontier Research Center (WPI-IFReC), Osaka University, Suita, Japan.
19. Department of Respiratory Medicine, Juntendo University Faculty of Medicine and Graduate School of Medicine, Tokyo, Japan.
20. Department of General Medicine, Juntendo University Faculty of Medicine and Graduate School of Medicine, Tokyo, Japan.
21. Department of Emergency and Disaster Medicine, Juntendo University Faculty of Medicine and Graduate School of Medicine, Tokyo, Japan.
22. Department of Cardiovascular Biology and Medicine, Juntendo University Faculty of Medicine and Graduate School of Medicine, Tokyo, Japan.
23. Department of Internal Medicine and Rheumatology, Juntendo University Faculty of Medicine and Graduate School of Medicine, Tokyo, Japan.
24. Department of Nephrology, Juntendo University Faculty of Medicine and Graduate School of Medicine, Tokyo, Japan.

ACCELERATED ARTICLE PREVIEW

25. Atopy (Allergy) Research Center, Juntendo University Graduate School of Medicine, Tokyo, Japan.
26. Department of Emergency and Critical Care Medicine, Keio University School of Medicine, Tokyo, Japan
27. Department of Anesthesiology, Keio University School of Medicine, Tokyo, Japan.
28. Department of Laboratory Medicine, Keio University School of Medicine, Tokyo, Japan
29. Keio University Health Center, Tokyo, Japan.
30. Department of Respiratory Medicine, Saitama Cardiovascular and Respiratory Center, Kumagaya, Japan.
31. JCHO (Japan Community Health care Organization) Saitama Medical Center, Internal Medicine, Saitama, Japan.
32. Department of Respiratory Medicine, Tokyo Women's Medical University, Tokyo, Japan.
33. Department of General Medicine, Tokyo Women's Medical University, Tokyo, Japan.
34. Clinical Research Center, Tokyo Medical and Dental University Hospital of Medicine, Tokyo, Japan.
35. Department of Medical Informatics, Tokyo Medical and Dental University Hospital of Medicine, Tokyo, Japan.
36. Respiratory Medicine, Tokyo Medical and Dental University, Tokyo, Japan.
37. Clinical Laboratory, Tokyo Medical and Dental University Hospital of Medicine, Tokyo, Japan.
38. Kawasaki Municipal Ida Hospital, Department of Internal Medicine, Kawasaki, Japan.
39. Department of Respiratory Medicine, Osaka Saiseikai Nakatsu Hospital, Osaka, Japan.
40. Department of Infection Control, Osaka Saiseikai Nakatsu Hospital, Osaka, Japan.
41. Department of Infectious Diseases, Tosei General Hospital, Seto, Japan.
42. Department of Respiratory Medicine and Allergy, Tosei General Hospital, Seto, Japan.
43. Department of Emergency and Critical Care Medicine, Kansai Medical University General Medical Center, Moriguchi, Japan.
44. Fukujuji hospital, Kiyose, Japan.
45. Department of Pulmonary Medicine, Saitama City Hospital, Saitama, Japan.
46. Department of Infectious Diseases, Saitama City Hospital, Saitama, Japan.
47. Department of General Thoracic Surgery, Saitama City Hospital, Saitama, Japan.
48. Department of Pulmonary Medicine, Eiju General Hospital, Tokyo, Japan.
49. Division of Infection Control, Eiju General Hospital, Tokyo, Japan.
50. Department of Hematology, Eiju General Hospital, Tokyo, Japan.
51. Saiseikai Utsunomiya Hospital, Utsunomiya, Japan.
52. Department of Respiratory Medicine, Tohoku University Graduate School of Medicine, Sendai, Japan
53. Department of Infectious Diseases, Tohoku University Graduate School of Medicine, Sendai, Japan
54. Department of Respiratory Medicine, Kitasato University Kitasato Institute Hospital, Tokyo, Japan.
55. Core Instrumentation Facility, Immunology Frontier Research Center and Research Institute for Microbial Diseases, Osaka University, Suita, Japan.
56. Laboratory of Human Immunology (Single Cell Immunology), Immunology Frontier Research Center, Osaka University, Suita, Japan.
57. Center for Infectious Disease Education and Research (CiDER), Osaka University, Suita, Japan.
58. Laboratory of Immune Regulation, Immunology Frontier Research Center, Osaka University, Suita, Japan.

ACCELERATED ARTICLE PREVIEW

59. Department of Pulmonary Medicine, Faculty of Medicine, University of Tsukuba, Tsukuba, Japan.
60. Department of Neurosurgery, Faculty of Medicine, the University of Tokyo, Tokyo, Japan.
61. Department of Integrative Physiology and Bio-Nano Medicine, National Defense Medical College, Tokorozawa, Japan.
62. Department of Otorhinolaryngology-Head and Neck Surgery, Osaka University Graduate School of Medicine, Suita, Japan.
63. Department of Head and Neck Surgery, Aichi Cancer Center Hospital, Nagoya, Japan
64. Department of Neurosurgery, Osaka University Graduate School of Medicine, Suita, Japan
65. Department of Otolaryngology and Head and Neck Surgery, Kansai Rosai Hospital, Hyogo, Japan
66. Division of Infection Control and Prevention, Osaka University Hospital, Suita, Japan.
67. Department of Biomedical Ethics and Public Policy, Osaka University Graduate School of Medicine, Suita, Japan.
68. Center for Genomic Medicine, Kyoto University Graduate School of Medicine, Kyoto, Japan.
69. Tachikawa Hospital, Tachikawa, Japan.
70. Department of Emergency and Critical Care Medicine, Tokyo Women's Medical University Medical Center East, Tokyo, Japan.
71. Department of Medicine, Tokyo Women's Medical University Medical Center East, Tokyo, Japan.
72. Department of Pediatrics, Tokyo Women's Medical University Medical Center East, Tokyo, Japan.
73. Internal Medicine, Sano Kosei General Hospital, Sano, Japan.
74. Japan Community Health care Organization Kanazawa Hospital, Kanazawa, Japan.
75. Department of Respiratory Medicine, Saiseikai Yokohamashi Nanbu Hospital, Yokohama, Japan.
76. Department of Clinical Laboratory, Saiseikai Yokohamashi Nanbu Hospital, Yokohama, Japan.
77. Internal Medicine, Internal Medicine Center, Showa University Koto Toyosu Hospital, Tokyo, Japan.
78. Department of Respiratory Medicine, Japan Organization of Occupational Health and Safety, Kanto Rosai Hospital, Kawasaki, Japan.
79. Department of General Internal Medicine, Japan Organization of Occupational Health and Safety, Kanto Rosai Hospital, Kawasaki, Japan.
80. Ishikawa Prefectural Central Hospital, Kanazawa, Japan.
81. Kanagawa Cardiovascular and Respiratory Center, Yokohama, Japan.
82. Department of Respiratory Medicine, National Hospital Organization Tokyo Medical Center, Tokyo, Japan.
83. Department of Allergy, National Hospital Organization Tokyo Medical Center, Tokyo, Japan.
84. Department of General Internal Medicine and Infectious Diseases, National Hospital Organization Tokyo Medical Center, Tokyo, Japan.
85. Department of Respiratory Medicine, Toyohashi Municipal Hospital, Toyohashi, Japan.
86. Keiyu Hospital, Yokohama, Japan.
87. KKR Sapporo Medical Center, Department of respiratory medicine, Sapporo, Japan.
88. Division of General Internal Medicine, Department of Internal Medicine, St. Marianna University School of Medicine, Kawasaki, Japan.

ACCELERATED ARTICLE PREVIEW

89. Department of Emergency and Critical Care Medicine, St.Marianna University School of Medicine, Kawasaki, Japan.
90. Japanese Red Cross Medical Center, Tokyo, Japan.
91. Matsumoto City Hospital, Matsumoto, Japan.
92. Department of Emergency and Critical Care Medicine, Faculty of Medicine, Fukuoka University, Fukuoka, Japan.
93. Department of Infection Control, Fukuoka University Hospital, Fukuoka, Japan.
94. Department of Rheumatology, National Hospital Organization Hokkaido Medical Center, Sapporo, Japan.
95. Department of Respiratory Medicine, National Hospital Organization Hokkaido Medical Center, Sapporo, Japan.
96. Department of Emergency and Critical Care Medicine, National Hospital Organization Hokkaido Medical Center, Sapporo, Japan.
97. National Hospital Organization Kanazawa Medical Center, Kanazawa, Japan.
98. Nihon University School of Medicine, Department of Internal Medicine, Division of Respiratory Medicine, Tokyo, Japan.
99. Musashino Red Cross Hospital, Musashino, Japan.
100. Division of Respiratory Medicine, Social Welfare Organization Saiseikai Imperial Gift Foundation, Inc., Saiseikai Kumamoto Hospital, Kumamoto, Japan.
101. Department of Respiratory Medicine, Nagoya University Graduate School of Medicine, Nagoya, Japan.
102. Fukuoka Tokushukai Hospital, Department of Internal Medicine, Kasuga, Japan.
103. Fukuoka Tokushukai Hospital, Respiratory Medicine, Kasuga, Japan.
104. Department of Endocrinology, Hematology and Gerontology, Chiba University Graduate School of Medicine, Chiba, Japan.
105. Department of Emergency and Critical Care Medicine, Chiba University Graduate School of Medicine, Chiba, Japan.
106. National Hospital Organization Kumamoto Medical Center, Kumamoto, Japan.
107. Division of Infectious Diseases and Respiratory Medicine, Department of Internal Medicine, National Defense Medical College, Tokorozawa, Japan.
108. Sapporo City General Hospital, Sapporo, Japan.
109. Department of Internal Medicine, Tokyo Saiseikai Central Hospital, Tokyo, Japan.
110. Department of Pulmonary Medicine, Tokyo Saiseikai Central Hospital, Tokyo, Japan.
111. Department of Respiratory Medicine, Fujisawa City Hospital, Fujisawa, Japan.
112. Uji-Tokushukai Medical Center, Uji, Japan.
113. Department of Infectious Disease and Clinical Research Institute, National Hospital Organization Kyushu Medical Center, Fukuoka Japan.
114. Department of Respirology, National Hospital Organization Kyushu Medical Center, Fukuoka, Japan.
115. Division of Respirology, Rheumatology, and Neurology, Department of Internal Medicine, Kurume University School of Medicine, Kurume, Japan.
116. Department of Infectious Disease, National Hospital Organization Kyushu Medical Center, Fukuoka Japan.
117. Ome Municipal General Hospital, Ome, Japan.
118. Research Institute for Diseases of the Chest, Graduate School of Medical Sciences, Kyushu University, Fukuoka, Japan.
119. Department of Medicine and Biosystemic Science, Kyushu University Graduate School of Medical Sciences, Fukuoka, Japan.
120. Daini Osaka Police Hospital, Osaka, Japan.

ACCELERATED ARTICLE PREVIEW

121. Department of Emergency and Critical Care Medicine, Faculty of Medicine, University of Tsukuba, Tsukuba, Japan.
122. Department of Hematology, Faculty of Medicine, University of Tsukuba, Tsukuba, Japan.
123. Department of Nephrology, Faculty of Medicine, University of Tsukuba, Tsukuba, Japan.
124. Department of Cardiovascular Surgery, Faculty of Medicine, University of Tsukuba, Tsukuba, Japan.
125. Division of Pulmonary Medicine, Department of Medicine, Tokai University School of Medicine, Isehara, Japan.
126. Department of Anesthesiology and Intensive Care Medicine, Kyoto Prefectural University of Medicine, Kyoto, Japan.
127. Department of Infection Control and Laboratory Medicine, Kyoto Prefectural University of Medicine, Kyoto, Japan.
128. Department of Respiratory Internal Medicine, St Marianna University School of Medicine, Yokohama Seibu Hospital, Yokohama, Japan.
129. KINSHUKAI Hanwa The Second Hospital, Osaka, Japan.
130. Gifu University School of Medicine Graduate School of Medicine, Emergency and Disaster Medicine, Gifu, Japan.
131. Department of Respiratory Medicine, Tokyo Medical University Hospital, Tokyo, Japan.
132. JA Toride medical hospital, Toride, Japan.
133. Okayama Rosai Hospital, Okayama, Japan.
134. Himeji St. Mary's Hospital, Himeji, Japan.
135. Emergency & Critical Care, Niigata University, Niigata, Japan.
136. Emergency & Critical Care Center, National Hospital Organization Kyoto Medical Center, Kyoto, Japan.
137. National Hospital Organization Tokyo Hospital Hospital, Kiyose, Japan.
138. Fujioka General Hospital, Fujioka, Japan.
139. Department of General Medicine, School of Medicine, International University of Health and Welfare Shioya Hospital, Ohtawara, Japan.
140. Department of Pharmacology, School of Pharmacy, International University of Health and Welfare, Ohtawara, Japan.
141. Department of Respiratory Medicine, International University of Health and Welfare Shioya Hospital, Ohtawara, Japan.
142. Department of Clinical Laboratory, International University of Health and Welfare Shioya Hospital, Ohtawara, Japan.
143. Department of Cardiology, Pulmonology, and Nephrology, Yamagata University Faculty of Medicine, Yamagata, Japan.
144. Division of Respiratory Medicine and Allergology, Department of Medicine, School of Medicine, Showa University, Tokyo, Japan.
145. Department of Pulmonary Medicine, Fukushima Medical University, Fukushima, Japan.
146. Kansai Electric Power Hospital, Osaka, Japan.
147. Department of Infectious Diseases, Kumamoto City Hospital, Kumamoto, Japan.
148. Department of Respiratory Medicine, Kumamoto City Hospital, Kumamoto, Japan.
149. Department of Emergency and Critical Care Medicine, Tokyo Metropolitan Police Hospital, Tokyo, Japan.
150. Department of Respiratory Medicine, Gunma University Graduate School of Medicine, Maebashi, Japan.
151. National hospital organization Saitama Hospital, Wako, Japan.
152. Tokyo Medical University Ibaraki Medical Center, Inashiki, Japan.
153. Department of Internal Medicine, Kiryu Kosei General Hospital, Kiryu, Japan.

ACCELERATED ARTICLE PREVIEW

154. Department of Pulmonary Medicine and Oncology,Graduate School of Medicine, Nippon Medical School, Tokyo, Japan
155. Division of Respiratory Medicine, Tsukuba Kinen General Hospital, Tsukuba, Japan.
156. Division of Respiratory Medicine, Department of Internal Medicine, Toho University Ohashi Medical Center, Tokyo, Japan.
157. Division of Anesthesiology, Department of Surgery Related, Kobe University Graduate School of Medicine, Kobe, Japan.
158. Genome Medical Science Project (Toyama), National Center for Global Health and Medicine, Tokyo, Japan.
159. School of Life Science and Technology, Tokyo Institute of Technology, Tokyo, Japan.
160. Laboratory of Viral Infection, Department of Infection Control and Immunology, Ōmura Satoshi Memorial Institute & Graduate School of Infection Control Sciences, Kitasato University, Tokyo, Japan.
161. Department of Insured Medical Care Management, Tokyo Medical and Dental University Hospital of Medicine, Tokyo, Japan.
162. Division of Immunogenetics, Department of Immunobiology and Neuroscience, Medical Institute of Bioregulation, Kyushu University, Fukuoka, Japan.
163. Department of Organoid Medicine, Keio University School of Medicine, Tokyo, Japan.
164. Medical Innovation Promotion Center, Tokyo Medical and Dental University, Tokyo, Japan.
165. Department of Surgery, Keio University School of Medicine, Tokyo, Japan.
166. Institute of Research, Tokyo Medical and Dental University, Tokyo, Japan.
167. Institute for the Advanced Study of Human Biology (WPI-ASHBi), Kyoto University, Kyoto, Japan.
168. Department of Medicine, Center for Hematology and Regenerative Medicine, Karolinska Institute, Stockholm, Sweden.
169. AMED-CREST, Japan Agency for Medical Research and Development, Tokyo, Japan.
170. Laboratory for Systems Genetics, RIKEN Center for Integrative Medical Sciences, Yokohama, Japan.
171. Laboratory of Statistical Immunology, Immunology Frontier Research Center (WPI-IFReC), Osaka University, Suita, Japan.
172. Department of Genome Informatics, Graduate School of Medicine, the University of Tokyo, Tokyo, Japan.
195. These authors contributed equally.
196. These authors jointly supervised the study.
* A list of authors and their affiliations appears at the end of the paper.

Corresponding to:

Koichi Fukunaga (kfukunaga@keio.jp), Division of Pulmonary Medicine, Department of Medicine, Keio University School of Medicine, Tokyo, Japan.

Yukinori Okada (yokada@sg.med.osaka-u.ac.jp), Department of Statistical Genetics, Osaka University Graduate School of Medicine, Suita, Japan.

ACCELERATED ARTICLE PREVIEW

Abstract

Identifying the factors underlying severe COVID-19 in the host genetics is an emerging issue[1–5]. We conducted a genome-wide association study (GWAS) involving 2,393 Japanese COVID-19 cases collected in initial pandemic waves with 3,289 controls, which identified a variant on 5q35 (rs60200309-A) near *DOCK2* associated with severe COVID-19 in younger (<65 ages) patients (n_{Case}=440, odds ratio=2.01, P=1.2×10^{-8}). This risk allele was prevalent in East Asians but rare in Europeans, showing a value of non-European GWAS. RNA-seq of 473 bulk peripheral blood identified decreasing effect of the risk allele on *DOCK2* expression in younger patients. *DOCK2* expression was suppressed in severe forms of COVID-19. Single cell RNA-seq analysis (n=61) identified cell type-specific downregulation of *DOCK2* and COVID-19-specific decreasing effects of the risk allele on *DOCK2* in non-classical monocytes. Immunohistochemistry of lung specimens from severe COVID-19 pneumonia showed suppressed DOCK2. Moreover, inhibition of DOCK2 function using CPYPP induced much severer pneumonia in a Syrian hamster model of SARS-CoV-2 infection characterized as weight loss, lung edema, enhanced viral loads, impaired macrophage recruitment and dysregulated type I interferon responses. DOCK2 plays a key role in host immune response to SARS-CoV-2 infection and development of severe COVID-19, being promising biomarker and therapeutic target.

(198 words)

ACCELERATED ARTICLE PREVIEW

Introduction

Coronavirus disease 2019 (COVID-19) caused by severe acute respiratory syndrome coronavirus 2 (SARS-CoV-2) is a serious global public health issue[6]. Although promising vaccines have recently become available, the emergence of SARS-CoV-2 variants may delay the end of this pandemic[7]. COVID-19 manifests a diverse clinical presentation from asymptomatic infection to fatal respiratory/multi-organ failure, in relation to multiple risk factors[8,9].

Human genetic background influences susceptibility to and/or severity of infectious diseases. The Severe Covid-19 genome-wide association study (GWAS) Group reported a variant at *LZTFL1* on 3p21 with severe COVID-19 risk in Europeans[1]. Of interest, these variants demonstrated globally heterogeneous allele frequency spectra, and were rarely present among East Asians[2].

Further GWAS efforts, including COVID-19 Human Genome Initiatives (HGI), have nominated host susceptibility genes[3–5]. However, the vast majority of existing studies were carried out on European populations. Considering global diversity of COVID-19 severity, COVID-19 host genetic analysis in non-Europeans should provide novel insights.

The Japan COVID-19 Task Force (JCTF) was established in early 2020 as a nation-wide multicenter consortium to overcome the COVID-19 pandemic in Japan (**Extended Data Fig. 1**, **Supplementary Table 1**). Here, we report the result of a large-scale GWAS of COVID-19 in Japanese with systemic comparisons to that in Europeans, which identified the population-specific risk allele at the *DOCK2* region conferring risk of severe COVID-19, especially in younger cases. We further conducted bulk and single cell transcriptomics, immunohistochemical assays of the COVID-19 patients and *in vivo* perturbation in a model organism. Our study found that *DOCK2* suppression is associated with the development of severe COVID-19 in a Syrian hamster model of SARS-CoV-2 infection, and that DOCK2-mediated signaling plays a key role in the host immune response to SARS-CoV-2 infection.

ACCELERATED ARTICLE PREVIEW

Results

Overview of the study participants

In the GWAS, we enrolled unrelated 2,393 patients with COVID-19 who required hospitalization from April 2020 to January 2021 (the 1st to 3rd pandemic waves in Japan), from >100 hospitals participating in JCTF. COVID-19 diagnoses of all cases were confirmed by physicians of each affiliated hospital based on clinical manifestations and a positive PCR test result. As for the control, we enrolled unrelated 3,289 subjects ahead of the COVID-19 pandemic who represent a general Japanese population. All the participants were confirmed to be of East Asian origin by a principal component analysis (**Extended Data Fig. 2a,b**).

Of the 2,393 COVID-19 cases, 990 ultimately had severe infection as defined by oxygen support, artificial respiration, and/or intensive-care unit hospitalization, while 1,391 cases had non-severe diseases. Severity information was not available for the remaining 12. As reported previously[8,10], the severe COVID-19 cases were relatively more aged (65.3 ± 13.9 years [mean ± SD]) and a higher proportion of males (73.9%), compared with non-severe cases (49.3 ± 19.2 years and 57.2% of males, respectively).

In the replication, we enrolled 1,243 severe COVID-19 cases collected from February 2021 to September 2021 (the 4th to 5th pandemic waves in Japan) and 3,769 controls. Detailed characteristics of the participants are in **Supplementary Table 2**.

COVID-19 GWAS in the Japanese population

The GWAS including all COVID-19 cases yielded no signals satisfying a genome-wide significance threshold ($P<5.0\times10^{-8}$; **Extended Data Fig. 2c**). Cross-population comparisons confirmed risk at multiple COVID-19-associated variants identified in the previous studies[1,3,5]. Seven out of the 11 reported-positive associations were replicated in our Japanese cohort with $P<0.05$, including those at *LZTFL1*, *FOXP4*, *TMEM65*, *ABO*, *TAC4*, *DPP9*, and *IFNAR2* (**Fig. 1a** and **Supplementary Table 3**), where the highest ORs were observed in comparisons for severe and younger COVID-19 cases a in six of the seven loci. The most significant replication was observed at *FOXP4*, as expected from its higher allele frequency in East Asians than in Europeans[3] (OR=1.29, 95% confidence interval [95%CI]=1.13-1.46, $P=9.1\times10^{-5}$ for severe COVID-19). By contrast, the risk allele at *LZTFL1* (rs35081325), which showed the strongest association in Europeans, was rare in Japanese. Despite its rare frequency (=0.0013 in controls), we nominally replicated the association with the highest risk in the severe and young COVID-19 (OR=11.8, 95%CI=1.64-85.5, $P=0.014$).

ACCELERATED ARTICLE PREVIEW

We evaluated the impact of HLA variants on COVID-19 risk[11,12] by *in silico* HLA imputation analysis[13,14]. We did not observe association signals satisfying the HLA-wide significance threshold (P<0.05/2,482 variants=2.0×10^{-5}; **Extended Data Fig. 3** and **Supplementary Table 4**). Among the four major ABO blood types[15], the O blood type was associated with a protective effect (P<0.05), most evidently in severe and younger cases (OR=0.73, 95%CI=0.56-0.93, P=0.014; **Extended Data Fig. 4a** and **Supplementary Table 5**)[1]. We found increased risk of the AB blood type, especially in severe cases (OR=1.41, 95%CI=1.10-1.81, P=0.0065 for all ages). The Japanese is the one with the highest AB blood type frequency[16] (=9.5% in our study), which might have provided power to detect its risk.

Cross-population Mendelian randomization

Next, to elucidate the medical conditions that can affect COVID-19 susceptibility, we applied cross-population two-sample Mendelian randomization (MR) analysis (**Supplementary Table 6**)[17]. In Japanese, as for severe COVID-19, a causal effect was inferred for obesity (P<0.0074; **Extended Data Fig. 4b** and **Supplementary Table 7**). We observed causal inference of asthma, uric acids (UA), and gout, while systemic lupus erythematosus (SLE) showed a protective effect (P<0.05). Hyperuricemia is a risk factors of severe COVID-19 in Japan[10], consistent with our MR findings. In Europeans, we observed significant causal inferences of obesity (P<6.2×10^{-6})[18], with doubled effect sizes in hospitalized and severe COVID-19 when compared with self-reported COVID-19. Our analysis provided additional evidence of obesity as a risk factor[8,9].

Population-specific risk allele at *DOCK2*

On the basis of the observation that many COVID-19 risk variants confer larger effects in severe and younger cases[1,3,5,19], we next performed the analysis by stratifying the subjects according to age and severity of the patients, where severe COVID-19 cases (n_{Case}=990), younger cases (ages<65, n_{Case}=1,484)[9], and their combinations (n_{Case}=440) were analyzed.

When comparison was made between younger cases with severe COVID-19 and respective controls, we identified a genetic locus on 5q35 that satisfied genome-wide significance (P =1.2×10^{-8} at rs60200309; **Fig. 1b**). The A allele of the lead SNP (rs60200309), located at an intergenic region downstream of *DOCK2*, was associated with an inflated risk for severe COVID-19 infection (OR=2.01, 95%CI=1.58-2.55, P=1.2×10^{-8}; **Table 1** and **Fig. 1c**). The risk rs60200309-A allele was also associated with an elevated risk of COVID-19 in other comparisons including all COVID-19 cases and controls (OR=1.24; **Supplementary**

ACCELERATED ARTICLE PREVIEW

Table 8, and also demonstrated within-case severity analysis (i.e., severe vs non-severe cases; OR=1.27 for all ages and OR=1.90 for ages<65).

We then conducted a replication study using additional 1,243 severe cases collected in the latter pandemic waves in Japan and 3,769 controls. We replicated an age-specific nominal risk in the younger COVID-19 cases (n_{Case}=833; OR=1.28, 95%CI=1.02-1.61, P=0.033; **Table 1**) compared to all ages (OR=1.00, 95%CI=0.85-1.19, P=0.96), while the effect size was smaller than observed in the GWAS cases collected in the initial pandemic waves. We note that decreased severity risk in latter pandemic waves was generally observed for other risk loci (e.g., from OR of 11.8 to 4.4 at *LZTFL1*; regression coefficient=0.57; **Extended Data Fig. 5**). This may suggest that longitudinal shifts of confounding factors along with pandemic waves, such as introduction of therapeutic strategies, high prevalence of vaccination, hospitalization policy changes, and virus strain evolutions, might have mitigated host genetics burdens defined in the initial pandemic waves, while further evaluations would be warranted.

We also looked up COVID-19 risk of the *DOCK2* variant in different ancestries (3,138 hospitalized COVID-19 cases vs 891,375 controls from the pan-ancestry meta-analysis)[20,21]. We observed the same directional effect with a marginal association signal (OR=1.73, 95%CI=0.95-3.15, P=0.072, $MAF_{Control}$=0.0008; **Supplementary Table 9**.

The variant was prevalent in East Asians (=0.097) with the highest frequency in Japanese (=0.125) and to a lesser extent in native Americans (=0.049), but very rare other ancestry (<0.005; **Fig. 1d**). Natural selection screening in Japanese[22] suggested marginal positive selection of the variant (P_{SDS}=0.051). Population-specific features of the *DOCK2* variant provide a rationale for COVID-19 host genetic researches in non-Europeans.

DOCK2 downregulation in severe COVID-19

To functionally annotate the *DOCK2* risk variant, we examined eQTL effect by conducting peripheral blood RNA-seq of the COVID-19 patients collected by JTCF (n=473). The risk allele at *DOCK2* (rs60200309-A) did not indicate a significant eQTL effect for all patients (β=-1.07, P=0.083; **Fig. 2a**). When stratified by the ages, a negative effect of the risk allele on *DOCK2* expression levels was observed for the younger patients (n=270; β=-2.15, P=0.0030 for ages <65). This allele did not show any significant eQTL on other surrounding genes (± 500kb window, P>0.070). We observed colocalization between the GWAS and the *DOCK2*

ACCELERATED ARTICLE PREVIEW

eQTL signals (colocalization posterior probability>0.01; **Extended Data Fig. 6** and **Supplementary Table 10**)[23].

We performed real-time qPCR-based DE analysis of *DOCK2* between severe and non-severe COVID-19 patients (n=468). We found decreased *DOCK2* expression (=*DOCK2*/*GAPDH*) in the severe patients (P=0.011; **Fig. 2b**). Suppression of *DOCK2* was clearer when stratified into younger patients (P=0.0068). When the patients were further stratified into asymptomatic, mild, severe, and most severe cases, negative correlation between *DOCK2* expression level and severity grades was observed (**Fig. 2c**). Taken together, *DOCK2* expression is downregulated in peripheral blood cells of severe COVID-19 patients, especially in the younger patients, and the risk variant might contribute to severe COVID-19 by suppressing expression of *DOCK2*.

DOCK2 (dedicator of cytokinesis 2) is a Rac activator involved in chemokine signaling, type I interferon (IFN) production, and lymphocyte migration[24,25]. Elucidation of immune cell-type specific expression profiles is necessary to disentangle roles of DOCK2 in the biology of COVID-19. We thus conducted single cell RNA sequencing (scRNA-seq) of peripheral blood mononuclear cells (PBMC) obtained from 30 severe COVID-19 cases and 31 healthy controls. We obtained 394,526 high-quality single cells and annotated 12 clusters (**Fig. 2d** and **Extended Data Fig. 7**). When projected, *DOCK2* expression was highest in $CD16^+$ monocytes (**Fig. 2e**). The percentage of cells expressing *DOCK2* was higher in innate immune cell clusters (monocytes and dendritic cells [DC]) (43.8%) than in other clusters (25.6%; **Fig. 2f**). DE analysis also demonstrated suppressed *DOCK2* expressions in the severe COVID-19 cases in the immune cell clusters as well (FC=0.82, P=8.3×10^{-4} for monocytes; FC=0.87, P=0.050 for DC; **Fig. 2g**).

To disentangle immune cell type specificity, we reconducted clustering and annotation by extracting 63,544 cells belonging to the innate cell clusters (**Fig. 2h** and **Extended Data Fig. 7**). Among the classified cell types (classical [$CD16^+CD14^{++}$], intermediate [$CD16^+CD14^+$], and non-classical [$CD16^{++}CD14^+$] monotypes, conventional dendritic cells [cDC] and plasmacytoid dendritic cells [pDC]), *DOCK2* expression was evidently high in the non-classical monocytes ($CD16^{++}CD14^+$ monocytes), of which involvement was implicated in the COVID-19 pathophysiology[26,27] (**Fig. 2h-j**). DE analysis showed the strongest downregulation of *DOCK2* in non-classical monocytes (FC=0.61, P=3.2×10^{-7}; **Fig. 2k**). *DOCK2* co-expression gene module[28] in non-classical monocytes of the COVID-19 cases implicated the enriched pathways such as immune response signaling pathways and phagocytosis (**Extended Data Fig. 7**). To consolidate evidence on variant-to-function, we

ACCELERATED ARTICLE PREVIEW

assessed single cell eQTL effect of the *DOCK2* risk variant. We found COVID-19 context-specific decreasing dosage effect of the risk variant on *DOCK2* expression in non-classical monocytes (β=-0.21, *P*=0.035 for COVID-19 and β=0.02, *P*=0.51 for controls; **Fig. 2l**).

We then evaluated biological impacts of *DOCK2* downregulation. In primary cell assays, *DOCK2* inhibition by CPYPP, a DOCK2-Rac1 interaction inhibitor[29], demonstrated reduced production of IFN-α of pDC under CpG stimulation (FC=5.5×10^{-5}, *P*=0.0038, *n*=3 per group; **Extended Data Fig. 8a**). pDC is another key innate immune cell involved in COVID-19 pathogenicity[30], where *DOCK2* expression was downregulated in COVID-19 cases (FC=0.79, *P*=0.019; **Fig. 2k**). Chemotaxis of $CD3^+$ T cells under CXCL12 stimulation was blocked (FC=0.57, *P*=1.0×10^{-7}, *n*=19 per group; **Extended Data Fig. 8b**). The *DOCK2* risk variant-phenotype link of IFN-α production in pDC and chemotaxis of $CD3^+$ T cells in primary cell assays was not significant (**Supplementary Fig. 1**). In THP-1 Blue ISG cells, *DOCK2* knockdown showed marked decrease in transcriptional activation of ISG, a surrogate of type I IFN (**Extended Data Fig. 8c-f** and **Supplementary Fig. 2**). These results highlight the important immunological roles of *DOCK2* in COVID-19 exacerbations such as type I IFN immunity and chemotaxis dysregulation, as exemplified by patients with congenital impairment in type I IFN immunity[31].

To confirm involvement of DOCK2 in COVID-19 pneumonia, we performed immunohistochemical analysis using autopsied human cadaver dead from COVID-19 (**Extended Data Fig. 9**). We examined 3 cases of COVID-19 pneumonia, and observed decreased expression of DOCK2 in lymphocytes and macrophages located in the lung and in hilar lymph node (Sample 1-3; **Fig. 2m**). In two control samples without pneumonia, we did not observe such decrease (Sample 4,5; **Fig. 2n**). DOCK2 was reported to be suppressed in bronchoalveolar lavage fluid (BALF) cells of COVID-19 patients[32], consistent with our findings. We observed loss of *DOCK2* expression in lymphocytes in the non-COVID-19 severe pneumonia case (Sample 6), while decrease of *DOCK2* expression was slightly observed in the non-COVID-19 mild pneumonia case (Sample 7). Thus, DOCK2 expression would be suppressed during severe pneumonia caused by COVID-19. These observations reveal linkage between cell type and tissue-specific downregulation of DOCK2, providing a potential value as a biomarker of severe COVID-19.

DOCK2 inhibition in Syrian hamster model

To decipher *in vivo* pathogenesis of *DOCK2* in COVID-19, we investigated the effects of DOCK2 suppression following SARS-CoV-2 infection using a Syrian hamster model

ACCELERATED ARTICLE PREVIEW

(**Extended Data Fig. 10a**)[33,34]. Administration of CPYPP (DOCK2 inhibitor) or vehicle (negative control) on mock infected animals did not induce weight loss (**Extended Data Fig. 10b**). When administrated with vehicle, animals infected with SARS-CoV-2 (*n*=12) showed weight loss to 83.3% by dpi 7, and then, the weights recovered up to 97.6% at dpi11. In contrast, when administrated with CPYPP, animals infected with SARS-CoV-2 (*n*=13) showed aberrant weight loss to 79.0% by dpi 7, and weight loss recover was restricted to 85.4% at dpi11 (**Fig. 3a** and **Extended Data Fig. 10c**). Advanced pulmonary edema was observed in lung of the CPYPP-administrated animals with SARS-CoV-2 infection (dpi 11; **Fig. 3b**). The largest lung weight (**Fig. 3c**) and the highest histopathological scoring changes of lung[34] (**Fig. 3d** and **Extended Data Fig. 10d-f**) were observed at dpi6. In lung immunohistochemistry, migration of CD68 macrophages around alveolar cells was impaired in the CPYPP-administrated animals with infection (**Fig. 3d** and **Extended Data Fig. 10e**). On the other hand, lung damage was mild or none at all in vehicle-administrated animals with infection or CPYPP-administrated animals without infection (**Fig. 3b-d** and **Extended Data Fig. 10d-f**).

Focusing on the deteriorating stages of SARS-CoV-2-induced pneumonia (dpi 3 and 6), we assayed SARS-CoV-2 viral loads in various organs. Increased viral loads were observed in nasal swab (dpi 3 and 6), lung (dpi 3), and intestine (dpi 6, $P<0.05$; **Fig. 3e**) of the CPYPP-administrated animals. Lung cytokine expression profile assay revealed that type I IFN (*IFN-α/β*) decreased at dpi 6 and type II IFN (*IFN-γ*) increased at dpi3 (**Fig. 3f**) under CPYPP administration. We also observed that CPYPP administration induced elevated inflammatory cytokine (*IL-6* at dpi3) and chemokine (C*CL5* at dpi3) levels. Roles of IFN response in pathogenicity of COVID-19 have been controversial[31,35,36]. Our observational and interventional findings on *DOCK2* downregulation proposed COVID-19 pneumonia pathophysiology where impaired macrophage recruitment at the site of infection and dysregulated IFN responses resulted in impaired virus elimination and prolonged lung inflammation.

ACCELERATED ARTICLE PREVIEW

Discussion

In this study, we reported GWAS of COVID-19 in Japanese, as one of the initial large-scale COVID-19 host genetic studies in non-Europeans. Our study not only confirmed the presence of multiple genetic variants associated with the COVID-19 risk shared across different populations, but also led the identification of a population-specific risk variant at *DOCK2*, particularly in younger cases with severe COVID-19 collected in the initial pandemic waves. Cross-population MR analysis disclosed a causal inference of a number of complex human traits on COVID-19, such as obesity. Our results highlight roles of the population-specific risk allele host genetic backgrounds, which underscores the need for non-European studies for COVID-19 host genetics. Of interest, autosomal recessive *DOCK2* deficiency is a Mendelian disorder with combined immunodeficiency and severe invasive pneumonia infection (OMIM:#616433)[37]. Our results should fulfill the genetic and clinical link between Mendelian disorders and common diseases. In the replication study using the cases collected in the latter pandemic waves, we observed significant but relatively smaller effect sizes of severe COVID-19 for the risk variants, including *DOCK2* and *LZTFL1*, identified in the studies based on the cases in the initial waves. How host genetics longitudinally interacts with confounding factors and affects COVID-19 phenotype spectra through the pandemic waves are still elusive. In the near future, a growing number of large-scale COVID-19 host genetics studies of diverse ancestry collection sites and period should be warranted, which contribute to guide a global health strategy against the pandemic.

Through the follow-up analyses of GWAS, we showed that DOCK2-mediated signaling plays a key role in the response to SARS-CoV-2 infection, suggesting that the hypomorphic *DOCK2* allele is involved in exacerbation of COVID-19, and that *DOCK2* could serve as a potential clinical biomarker predicting severe COVID-19. Bulk and single cell transcriptome analysis of peripheral blood cells identified cell type-specific downregulation of *DOCK2* modulated by COVID-19-specific eQTL effect of the *DOCK2* risk variant in patients with severe COVID-19, which was most evident in innate immune cells including non-classical monocytes and pDC. Nevertheless, causal inference of the COVID-19-specific eQTL on COVID-19 severity could be circular. Potentially, the risk variant induces *DOCK2* downregulation in early phase of infection. Immunohistochemical analysis showed suppressed DOCK2 in lung of COVID-19 pneumonia. *In vivo* suppression of DOCK2 by CPYPP following SARS-CoV-2 infection in the Syrian hamster model resulted in severe COVID-19 pneumonia highlighted as impaired migration of macrophages and dysregulation of IFN response. We note the possibility that CPYPP is not specific to DOCK2 and inhibits

ACCELERATED ARTICLE PREVIEW

664 other DOCK family genes. Alternatively, *DOCK2* boosting assays are warranted to ideally
665 provide an evidence of its role in COVID-19 pathophysiology. Taken together with its critical
666 roles of in immune regulations[25], upregulation of DOCK2 is considered as potential
667 therapeutic strategy of COVID-19. Our results motivate us for further studies linking DOCK2
668 to COVID-19 molecular and clinical phenotypes toward our challenge to overcome the
669 pandemic.
670

ACCELERATED ARTICLE PREVIEW

References

1. The Severe Covid-19 GWAS Group. Genomewide Association Study of Severe Covid-19 with Respiratory Failure. *N. Engl. J. Med.* **383**, 1522–1534 (2020).
2. Zeberg, H. & Pääbo, S. The major genetic risk factor for severe COVID-19 is inherited from Neanderthals. *Nature* **587**, 610–612 (2020).
3. Niemi, M. E. K. *et al.* Mapping the human genetic architecture of COVID-19. *Nature* **600**, 472–477 (2021).
4. Kosmicki, J. A. *et al.* Pan-ancestry exome-wide association analyses of COVID-19 outcomes in 586,157 individuals. *Am. J. Hum. Genet.* **108**, 1350–1355 (2021).
5. Pairo-Castineira, E. *et al.* Genetic mechanisms of critical illness in COVID-19. *Nature* **591**, 92–98 (2021).
6. Zhu, N. *et al.* A Novel Coronavirus from Patients with Pneumonia in China, 2019. *N. Engl. J. Med.* **382**, 727–733 (2020).
7. Walensky, R. P., Walke, H. T. & Fauci, A. S. SARS-CoV-2 Variants of Concern in the United States-Challenges and Opportunities. *JAMA - J. Am. Med. Assoc.* **325**, 1037–1038 (2021).
8. Williamson, E. J. *et al.* Factors associated with COVID-19-related death using OpenSAFELY. *Nature* **584**, 430–436 (2020).
9. Ministry of Health Labour and Welfare. Clinical Management of Patients with COVID-19 A guide for front-line. (2020).
10. Ishii, M. *et al.* Clinical characteristics of 345 patients with coronavirus disease 2019 in Japan: A multicenter retrospective study. *J. Infect.* **81**, e3–e5 (2020).
11. Nguyen, A. *et al.* Human Leukocyte Antigen Susceptibility Map for Severe Acute Respiratory Syndrome Coronavirus 2. *J. Virol.* **94**, 1–12 (2020).
12. Ben Shachar, S. *et al.* MHC Haplotyping of SARS-CoV-2 Patients: HLA Subtypes Are Not Associated with the Presence and Severity of COVID-19 in the Israeli Population. *J. Clin. Immunol.* **41**, 1154–1161 (2021).
13. Hirata, J. *et al.* Genetic and phenotypic landscape of the major histocompatibilty complex region in the Japanese population. *Nat. Genet.* **51**, 470–480 (2019).
14. Naito, T. *et al.* A deep learning method for HLA imputation and trans-ethnic MHC fine-mapping of type 1 diabetes. *Nat. Commun.* **12**, 1639 (2021).
15. Lane, W. J. *et al.* Automated typing of red blood cell and platelet antigens: a whole-genome sequencing study. *Lancet Haematol.* **5**, e241–e251 (2018).
16. Liu, Y., Häussinger, L., Steinacker, J. M. & Dinse-Lambracht, A. Association between the dynamics of the COVID-19 epidemic and ABO blood type distribution. *Epidemiol. Infect.* **149**, e19 (2021).
17. Holmes, M. V., Ala-Korpela, M. & Smith, G. D. Mendelian randomization in cardiometabolic disease: Challenges in evaluating causality. *Nat. Rev. Cardiol.* **14**, 577–599 (2017).
18. Freuer, D., Linseisen, J. & Meisinger, C. Impact of body composition on COVID-19 susceptibility and severity: A two-sample multivariable Mendelian randomization study. *Metabolism.* **118**, 154732 (2021).

ACCELERATED ARTICLE PREVIEW

19. Nakanishi, T. *et al.* Age-dependent impact of the major common genetic risk factor for COVID-19 on severity and mortality. *J. Clin. Invest.* **131**, 2021.03.07.21252875 (2021).
20. Roberts, G. H. L. *et al.* AncestryDNA COVID-19 host genetic study identifies three novel loci. *medRxiv* 2020.10.06.20205864 (2020) doi:10.1101/2020.10.06.20205864.
21. Roberts, G. H. *et al.* Novel COVID-19 phenotype definitions reveal phenotypically distinct patterns of genetic association and protective effects 2 3. *medRxiv* 2021.01.24.21250324 (2021) doi:10.1101/2021.01.24.21250324.
22. Okada, Y. *et al.* Deep whole-genome sequencing reveals recent selection signatures linked to evolution and disease risk of Japanese. *Nat. Commun.* **9**, 1–10 (2018).
23. Hormozdiari, F. *et al.* Colocalization of GWAS and eQTL Signals Detects Target Genes. *Am. J. Hum. Genet.* **99**, 1245–1260 (2016).
24. Fukui, Y. *et al.* Haematopoietic cell-specific CDM family protein DOCK2 is essential for lymphocyte migration. *Nature* **412**, 826–831 (2001).
25. Nishikimi, A. *et al.* Sequential regulation of DOCK2 dynamics by two phospholipids during neutrophil chemotaxis. *Science (80-.).* **324**, 384–387 (2009).
26. Stephenson, E. *et al.* Single-cell multi-omics analysis of the immune response in COVID-19. *Nat. Med.* **27**, 904–916 (2021).
27. Ahern, D. J. *et al.* A blood atlas of COVID-19 defines hallmarks of disease severity and specificity. *Cell* 916–938 (2022) doi:10.1016/j.cell.2022.01.012.
28. Langfelder, P. & Horvath, S. WGCNA: An R package for weighted correlation network analysis. *BMC Bioinformatics* **9**, (2008).
29. Nishikimi, A. *et al.* Blockade of Inflammatory Responses by a Small-Molecule Inhibitor of the Rac Activator DOCK2. *Chem. Biol.* **19**, 488–497 (2012).
30. Saichi, M. *et al.* Single-cell RNA sequencing of blood antigen-presenting cells in severe COVID-19 reveals multi-process defects in antiviral immunity. *Nat. Cell Biol.* **23**, 538–551 (2021).
31. Zhang, Q. *et al.* Inborn errors of type I IFN immunity in patients with life-threatening COVID-19. *Science (80-.).* **370**, eabd4570 (2020).
32. Zhou, Z. *et al.* Heightened Innate Immune Responses in the Respiratory Tract of COVID-19 Patients. *Cell Host Microbe* **27**, 883-890.e2 (2020).
33. Ebisudani, T. *et al.* Report Direct derivation of human alveolospheres for SARS- CoV-2 infection modeling and drug screening ll Direct derivation of human alveolospheres for SARS-CoV-2 infection modeling and drug screening. *CellReports* **35**, 109218 (2021).
34. Imai, M. *et al.* Syrian hamsters as a small animal model for SARS-CoV-2 infection and countermeasure development. *Proc. Natl. Acad. Sci.* **117**, 16587–16595 (2020).
35. Yoshida, M. *et al.* Local and systemic responses to SARS-CoV-2 infection in children and adults. *Nature* **602**, (2021).
36. Loske, J. *et al.* Pre-activated antiviral innate immunity in the upper airways controls early SARS-CoV-2 infection in children. *Nat. Biotechnol.* (2021) doi:10.1038/s41587-021-01037-9.
37. Dobbs, K. *et al.* Inherited DOCK2 Deficiency in Patients with Early-Onset Invasive Infections. *N. Engl. J. Med.* **372**, 2409–2422 (2015).

ACCELERATED ARTICLE PREVIEW

Acknowledgements

We would like to sincerely thank all the participants involved in this study, and all the members of JCTF for their supports. We thank Mr. Johji Kitano, e-Parcel Corporation, and Ascend Corporation for voluntarily supporting JCTF. We thank COVID-19 Host Genetics Initiative for publicly sharing the GWAS summary statistics. This study was supported by AMED (JP20nk0101612, JP20fk0108415, JP21jk0210034, JP21km0405211, JP21km0405217, JP21fk0108469, JP21wm0325031, JP21gm4010006, JP22km0405211, JP22ek0410075, JP22km0405217, JP22ek0109594), JST CREST (JPMJCR20H2), JST PRESTO (JPMJPR21R7), JST Moonshot R&D (JPMJMS2021, PMJMS2024), MHLW (20CA2054), JSPS KAKENHI (22H00476), Takeda Science Foundation, the Mitsubishi Foundation, the Team Osaka University Research Project in The Nippon Foundation - Osaka University Project for Infectious Disease Prevention, and Bioinformatics Initiative of Osaka University Graduate School of Medicine. The super-computing resource was provided by Human Genome Center (the Univ. of Tokyo).

Author contributions

Y.O. and K.F. supervised the study. H.N., R.E. T.T., H.N., T.U., K.K., M.A., Y.F., A.K., T.S., N.H., K.T., M.I., R.K., Y.K., A.K., S.I., S.M., S.O., T.K., K.F. and Y.O. designed the study. H.N., R.E., T.T., H.N., Y.S., K.S., H.T., S.A., Y.M., H.L., T.H., K.O., D.O., D.M., M.K., T.N., K.Y., Q.S.W., R.S., R.I., Y.M., J.H., A.K., S.I., S.M., S.O., T.K., K.F. and Y.O. wrote the manuscript. H.N., R.E., T.T., H.N., Y.S., K.S., H.T., S.A., Y.M., H.L., T.H., K.O., D.O., D.M., M.K., T.N., K.Y., Q.S.W., R.S., R.I., Y.M., J.H., H.H., Y.Y., N.T., E.Y., T.H., E.S., K.K., Y.K., T.M., A.K., S.I., S.M., S.O., T.K., K.F. and Y.O. conducted data analysis. H.N., R.E., T.T., H.N., Y.S., K.S., H.T., S.A., Y.M., H.L., T.H., K.O., D.O., D.M., M.K., T.N., K.Y., Q.S.W., R.S., R.I., Y.M., J.H., H.H., Y.Y., N.T., E.Y., T.H., E.S., K.K., Y.K., T.M., Y.N., T.U., K.K., M.A., Y.F., A.K., T.S., N.H., K.T., M.I., R.K., Y.K., A.K., S.I., S.M., S.O., T.K., K.F. and Y.O. collected data. All other authors collected samples.

Competing interests

The authors declare no conflicts of interests.

The Biobank Japan Project

Koichi Matsuda[173,174], Yuji Yamanashi[175], Yoichi Furukawa[176], Takayuki Morisaki[177], Yoshinori Murakami[178], Yoichiro Kamatani[179,174], Kaori Muto[180], Akiko Nagai[180], Wataru

ACCELERATED ARTICLE PREVIEW

Obara[181], Ken Yamaji[182], Kazuhisa Takahashi[19], Satoshi Asai[183,184], Yasuo Takahashi[184], Takao Suzuki[185], Nobuaki Sinozaki[185], Hiroki Yamaguchi[186], Shiro Minami[187], Shigeo Murayama[188], Kozo Yoshimori[189], Satoshi Nagayama[190], Daisuke Obata[191], Masahiko Higashiyama[192], Akihide Masumoto[193], Yukihiro Koretsune[194]

173. Laboratory of Genome Technology, Human Genome Center, Institute of Medical Science, The University of Tokyo, Tokyo, Japan.

174. Laboratory of Clinical Genome Sequencing, Graduate School of Frontier Sciences, The University of Tokyo, Tokyo, Japan.

175. Division of Genetics, The Institute of Medical Science, The University of Tokyo, Tokyo, Japan.

176. Division of Clinical Genome Research, Institute of Medical Science, The University of Tokyo, Tokyo, Japan.

177. Division of Molecular Pathology, IMSUT Hospital Department of Internal Medicine, Institute of Medical Science, The University of Tokyo, Tokyo, Japan.

178. Department of Cancer Biology, Institute of Medical Science, The University of Tokyo, Tokyo, Japan.

179. Laboratory of Complex Trait Genomics, Graduate School of Frontier Sciences, The University of Tokyo, Tokyo, Japan.

180. Department of Public Policy, Institute of Medical Science, The University of Tokyo, Tokyo, Japan.

181. Department of Urology, Iwate Medical University, Iwate, Japan.

182. Department of Internal Medicine and Rheumatology, Juntendo University Graduate School of Medicine, Tokyo, Japan.

183. Division of Pharmacology, Department of Biomedical Science, Nihon University School of Medicine, Tokyo, Japan.

184. Division of Genomic Epidemiology and Clinical Trials, Clinical Trials Research Center, Nihon University. School of Medicine, Tokyo, Japan.

185. Tokushukai Group, Tokyo, Japan.

186. Departmentof Hematology, Nippon Medical School, Tokyo, Japan

187. Department of Bioregulation, Nippon Medical School, Kawasaki, Japan.

188. Tokyo Metropolitan Geriatric Hospital and Institute of Gerontology, Tokyo, Japan.

189. Fukujuji Hospital, Japan Anti-Tuberculosis Association, Tokyo, Japan.

190. The Cancer Institute Hospital of the Japanese Foundation for Cancer Research, Tokyo, Japan.

191. Center for Clinical Research and Advanced Medicine, Shiga University of Medical Science, Shiga, Japan.

192. Department of General Thoracic Surgery, Osaka International Cancer Institute, Osaka, Japan.

193. IIZUKA HOSPITAL, Fukuoka, Japan.

ACCELERATED ARTICLE PREVIEW

833 194. National Hospital OrganizationOsaka National Hospital, Osaka, Japan.

834

835

ACCELERATED ARTICLE PREVIEW

Main Figure legends

Figure 1. Severe and younger COVID-19 GWAS in the Japanese population

(**a**) Forest plots of the risk of COVID-19-associated variants in Japanese. Odds ratios of the COVID-19-associated variants in the Japanese population are indicated. (**b**) A Manhattan plot of the severe and younger COVID-19 GWAS (440 cases and 2,377 controls). Uncorrected *P* values from GWAS analysis are shown. A dotted line represents the genome-wide significance threshold of $P < 5.0\times10^{-8}$. Manhattan and quantile-quantile plots of all GWAS results are in **Extended Data Fig. 2**. (**c)** A regional association plot at the *DOCK2* locus. Dots represent SNPs with colors according to linkage disequilibrium (r^2) with the lead SNP of rs60200309. (**d**) Allele frequency spectra of the rs60200309-A allele in the 1000 Genomes Project Phase3v5 database.

Figure 2. Cell type and tissue-specific expression profile of *DOCK2* and its down-regulation in severe COVID-19

(**a**) eQTL effect of the COVID-19 risk variant (rs60200309) on *DOCK2* expression levels, measured as TPM using bulk RNA-seq of peripheral blood. The risk allele (rs60200309-A) decreases *DOCK2* levels in cases with ages<65. (**b,c**) *DOCK2* differential expression analysis on COVID-19 severity. *DOCK2* expression levels were quantified by qPCR and adjustment with GAPDH. (**b**) Comparison between severe and non-severe COVID-19 cases. (**c**) Comparison among the most severe, severe, mild, and asymptomatic cases of COVID-19. (**d-k**) Results of the PBMC scRNA sequence of severe cases of COVID-19 (*n*=30) and healthy controls (*n*=31). (**d**) UMAP visualization of all 394,526 cells. (**e**) Projection of gene expression density of *DOCK2*. Innate immune cell clusters are framed by a red dotted rectangle. (**f**) Percentages of *DOCK2* expressing cells and their expression levels, and (**g**) expression changes in differential expression analysis are indicated for six major cell types. (**h**) Visualization and annotation of the innate immune cell clusters. (**i-k**) *DOCK2* expression and its expression changes in differential expression analysis in the innate immune cell clusters, corresponding to (**e-g**). (**l**) COVID-19 context-specific decreasing eQTL effect of the *DOCK2* risk variant at non-classical monocytes. (**m,n**) Immunohistochemical analysis for DOCK2. Lung and hilar lymph nodes were obtained from COVID-19 pneumonia (Sample 1; left panel) and control (Sample 5; right panel), and stained with anti-DOCK2 polyclonal antibody. The results of all the samples (Sample 1-7) are in **Extended Data Fig. 9**. In (**a-c**)

ACCELERATED ARTICLE PREVIEW

and (**l**), boxes denote the interquartile range (IQR), and the median is shown as horizontal bars. Whiskers extend to 1.5 times the IQR, and outliers are shown as individual points in (**a-c**) and all samples are shown as individual points in (**l**). Uncorrected *P* values are shown in (**a-c, g, k-l**).

Figure 3. ***In vivo suppression of*** **DOCK2 in a Syrian hamster model with SARS-CoV-2 infection**

(**a**) Changes in weight of animals infected with SARS-CoV-2. (**b**) Representative photographic image of the lung sample, collected after euthanizing the animals at dpi 11. (**c**) Lung weight changes after infection. (**d**) Representative lung histopathology and immunohistochemistry of the infected animals at dpi 6. Middle and Right of histopathology show enlarged views of the area circled in black in Left. (Scale bars, 2.5 mm [Left], 1.0 mm [Middle], and 0.25 mm [Right].) In immunohistochemistry for alveolar macrophage, lung tissue was stained with the anti-CD68 mouse monoclonal antibody. (Scale bars, 0.25 mm.) (**e**) SARS-CoV-2 viral loads at the organs of the infected animals. (**f**) Lung cytokine expression assays of the infected animals. In (**a**) and (**c**), the error bars represent standard error of the mean, and *P* values were determined with two-sided Welch's *t*-test; **P*<0.05; ***P*<0.01; ****P*<0.001. In (**e**) and (**f**), boxes denote the interquartile range (IQR), and the median is shown as horizontal bars. Whiskers extend to 1.5 times the IQR, and all animals are shown as individual points. *P* values were determined with two-sided Wilcoxon rank sum test.

ACCELERATED ARTICLE PREVIEW

Methods

Study participants

All the cases affected with COVID-19 were recruited through JCTF. We enrolled the hospitalized cases diagnosed as COVID-19 by physicians using the clinical manifestation and PCR test results, who were recruited at any of the >100 the affiliated hospitals from April 2020 to January 2021 (for the GWAS) or from February 2021 to September 2021 (for the replication; **Supplementary Table 1 and 2**). Patients requiring oxygen support, artificial respiration, and/or intensive-care unit (ICU) hospitalization were defined as 'severe COVID-19', while others were defined as 'non-severe COVID-19'. Details of the clinical manifestation including cardiovascular and respiratory comorbidities are provided in **Supplementary Table 2**. The threshold of 65 years of age was selected according to the clinical management guide in Japan[9]. Control subjects were collected as general Japanese populations at Osaka University and affiliated institutes (for the GWAS and replication) or by the Biobank Japan Project[38] (for the replication). Individuals determined to be of non-Japanese origin either of self-reporting or by principal component analysis were excluded as described elsewhere (**Extended Data Fig. 2a**)[39]. All the participants provided written informed consent as approved by the ethical committees of the affiliated institutes (Keio IRB approval #20200061).

GWAS genotyping and quality control

We performed GWAS genotyping of the 2,520 COVID-19 cases and 3,341 controls using Infinium Asian Screening Array (Illumina, USA). We applied stringent quality control (QC) filters to the samples (sample call rate < 0.97, excess heterozygosity of genotypes > mean + 3SD, related samples with PI_HAT > 0.175, or outlier samples from East Asian clusters in principal component analysis with 1000 Genomes Project samples), and variants (variant call rate < 0.99, significant call rate differences between cases and controls with $P < 5.0\times10^{-8}$, deviation from Hardy-Weinberg equilibrium with $P < 1.0\times10^{-6}$, or minor allele count < 5). Details of the QC for the mitochondrial variants are described elsewhere[40]. After QC, we obtained genotype data of 489,539, 15,161, and 217 autosomal, X-chromosomal, and mitochondrial variants, respectively, for 2,393 COVID-19 cases and 3,289 controls.

Genome-wide genotype imputation

We used SHAPEIT4 software (version 4.1.2) for haplotype phasing of autosomal genotype data, and SHAPEIT2 software (v2.r904) for X-chromosomal genotype data. After phasing, we used Minimac4 software (version 1.0.1) for genome-wide genotype imputation. We used

ACCELERATED ARTICLE PREVIEW

the population-specific imputation reference panel of Japanese (n = 1,037) combined with 1000 Genomes Project Phase3v5 samples (n = 2,504)[22]. Imputations of the mitochondrial variants were conducted as described elsewhere[40], using the population-specific reference panel (n = 1,037). We applied post-imputation QC filters of MAF ≥ 0.1% and imputation score (Rsq) > 0.5, and obtained 13,116,003, 368,566 and 554 variants for autosomal, X-chromosomal, and mitochondrial variants, respectively. We note that the genotypes of the lead variant in the GWAS (rs60200309) were obtained by imputation (Rsq = 0.88). We assessed accuracy by comparing the imputed dosages with WGS data for the part of the controls (n = 236), and confirmed high concordance rate of 97.5%.

Case-control association test

We conducted GWAS of COVID-19 by using logistic regression of the imputed dosages of each of the variants on case-control status, using PLINK2 software (v2.00a3LM AVX2 Intel [6 Jul 2020]). We included sex, age, and the top 5 principal components as covariates in the regression model. We set the genome-wide association significance threshold of $P < 5.0\times10^{-8}$.

HLA genotype imputation and association test

HLA genotype imputation was performed using DEEP*HLA software (version 1.0), a multitask convolutional deep learning method[14]. We used the population-specific imputation reference panel of Japanese (n = 1,118), which included both classical and non-classical HLA gene variants for imputation[13]. Before imputation, we removed the overlapping samples between the GWAS controls and the reference panel (n = 649), from the GWAS data side. We imputed HLA alleles (2-digit and 4-digit) and the corresponding HLA amino acid polymorphisms, and applied post-imputation QC filters of MAF ≥ 0.5% and imputation score (r^2 in cross-validation) > 0.7.

As for the imputed HLA variants, we conducted (i) association test of binary HLA markers (2-digit and 4-digit HLA alleles, respective amino acid residues) and (ii) an omnibus test of each of the HLA amino acid positions, as described elsewhere[13]. Binary maker test was conducted using the same logistic regression model and covariates as in the GWAS. Omnibus test was conducted by a log likelihood ratio test between the null model and the fitted model, followed by a χ^2 distribution with m-1 degree(s) of freedom, where m is the number of the residues. R statistical software (version 3.6.0) was used for the HLA

ACCELERATED ARTICLE PREVIEW

association test. We set the HLA-wide significance threshold based on Bonferroni's correction for the number of the HLA tests (α = 0.05).

Estimation of the ABO blood types and analysis

We estimated the ABO blood types of the GWAS subjects based on the five coding variants at the *ABO* gene (rs8176747, rs8176746, rs8176743, rs7853989, and rs8176719)[41]. We phased the haplotypes of these five variants based on the best-guess genotypes obtained by genome-wide imputation, and estimated the ABO blood type as described elsewhere[15]. We could unambiguously determine the ABO blood type of 99.1 % of the subjects.

Blood group-specific ORs were estimated based on comparisons of A vs AB/B/O, B vs A/AB/O, AB vs A/B/O, and O vs A/AB/B. We conducted a logistic regression analysis including age, sex and the top 5 principal components as covariates. *R* statistical software (version 3.6.3) was used for the ABO blood type analysis.

Cross-population MR analysis

We conducted two-sample MR analysis as described elsewhere[17,42]. As exposure, we selected a series of clinical states where altered comorbidity with COVID-19 have been discussed. As an outcome phenotype, we utilized the GWAS summary statistics of Japanese (current study) and Europeans (release 5 from COVID-19 HGI[3]). Lists of the Japanese and European GWAS studies used as the exposure phenotypes are in **Supplementary Table 6**. We extracted the independent lead variants with genome-wide significance (or the proxy variants in linkage disequilibrium $r^2 \geq 0.8$ in the EAS or EUR subjects of the 1000 Genomes Project Phase3v5 databases) from the GWAS results of the exposure phenotypes. We applied the inverse variance weighted (IVW) method using the TwoSampleMR package (version 0.5.5) in R statistical software (version 4.0.2).

The replication analysis

We genotyped additional 1,243 severe COVID-19 cases and 3,769 controls using Infinium Asian Screening Array (Illumina, USA). We applied the QC filters and genotype imputation, and conducted case-control analysis of the variant as in the same manner as the GWAS.

RNA-seq of peripheral blood of the COVID-19 patients

We incorporated 475 COVID-19 patients collected at the core medical institutes of JCTF and included in the GWAS for the bulk RNA-seq analysis (**Supplementary Table 2**). Isolation of

ACCELERATED ARTICLE PREVIEW

RNA from the peripheral blood of the COVID-19 patients was conducted using RNeasy Mini Kit (Qiagen, USA). Libraries for RNA-seq were prepared using NEBNext® Poly(A) mRNA Magnetic Isolation Module and NEBNext® Ultra™ Directional RNA Library Prep Kit for Illumina (New England BioLabs, USA). RNA-seq was performed using the NovaSeq6000 platform (Illumina, USA) with paired end reads (read length of 100 bp), using S4 Reagent kit (200 cycles). We obtained on average 71,724,142±17,527,007 reads per a sample (mean±SD). Sequencing reads were quality-filtered, and adapter removal was performed using the Trimmomatic (v0.39)[43]. Alignment to the human reference genome GRCh38/hg38 was performed using STAR (v2.7.9a)[44], based on the GENCODE v30 annotation. Gene level quantification and normalization was using RSEM (v1.3.3)[45]. Transcripts per kilobase million (TPM) was used as an index of gene quantification. We excluded the two outlier samples in the PCA plot of the TPM from the analysis (n = 473 for the analysis). We quantified 58,825 genes, and adopted the 5,991 genes with the median TPM > 10 for the subsequent analysis.

In the eQTL analysis of the *DOCK2* variant, dosage effects of the risk variant (rs60200309-A) on the gene expression levels (TPM) were evaluated using linear regression models with age, sex, severity, the top 10 PCs of the TPM matrix, and the top 5 PCs of the GWAS data as covariates. The dosage effects of the risk variant on the expression of nearby genes located within a 500kb window were also evaluated. *R* statistical software (version 3.6.3) was used for the analysis. Colocalization analysis between the GWAS and the *DOCK2* eQTL signals was conducted using eCAVIAR[23].

qPCR-based DE analysis on COVID-19 severity

Real-time qPCR was conducted for the RNA isolated from the peripheral blood of the COVID-19 patients (n = 468). Total RNA was reverse-transcribed using the High-Capacity RNA-to-cDNA cDNA Kit (Life Technologies). Real-time qPCR was performed using TaqMan® assays on a 7500 Fast Real-Time PCR system (Applied Biosystems; probe assay ID: Hs00386045_m1 [*DOCK2*] and Hs99999905_m1 [*GAPDH*]). DE analysis was conducted between severe and non-severe COVID-19, and across four COVID-19 disease severity grades, ordered from Asymptomatic > Mild > Severe > Most Severe. Among the severe COVID-19, patients in ICU or requiring intubation and ventilation were defined as 'Most Severe' disease, while the rest as 'Severe' disease. Among the non-severe COVID-19, patients without any symptoms related to COVID-19 were defined as 'Asymptomatic' disease, while others as 'Mild' disease. The analysis was performed on relative messenger RNA

ACCELERATED ARTICLE PREVIEW

expression revel of *DOCK2* adjusted with *GAPDH* (= *DOCK2*/*GAPDH*) using linear regression models with age and sex as covariates in *R* statistical software (version 3.6.3).

Subjects and specimen collection of PBMC for scRNA-seq

Peripheral blood samples were obtained from severe COVID-19 patients (*n* =30) and healthy controls (*n* = 31) collected at Osaka University Graduate School of Medicine. Of the 30 COVID-19 patients, 5 patients were classified as moderate and 25 patients as severe according to disease severity based on the highest score on the World Health Organization (WHO) Ordinal Scale for Clinical Improvement ever present (WHO. R&D Blueprint - novel Coronavirus - COVID-19 Therapeutic Trial Synopsis. 2020.). For both patients with COVID-19 and healthy controls, blood was collected into heparin tubes and PBMCs were isolated using Leucosep (Greiner Bio-One) density gradient centrifugation according to the manufacturer's instructions. Blood was processed within 3 h of collection for all samples, and stored at -80 °C until use.

Droplet-based single-cell sequencing

Single-cell suspension were processed through the 10x Genomics Chromium Controller (10x Genomics, USA) following the protocol outlined in the Chromium Single Cell V(D)J Reagent Kits (v1.1 Chemistry) User Guide. Chromium Next GEM Single Cell 5' Library & Gel Bead Kit v1.1 (Cat# PN-1000167), Chromium Next GEM Chip G Single Cell Kit (Cat# PN-1000127) and Single Index Kit T Set A (Cat# PN-1000213) were applied during the process. Approximately 16,500 live cells per sample were separately loaded into each port of the Chromium controller without sample mixing to generate 10,000 single-cell gel-bead emulsions for library preparation and sequencing, according to the manufacturer's recommendations. Oil droplets of encapsulated single cells and barcoded beads (GEMs) were subsequently reverse-transcribed in a Veriti Thermal Cycler (Thermo Fisher Scientific), resulting in cDNA tagged with a cell barcode and unique molecular index (UMI). Next, cDNA was then amplified to generate single-cell libraries according to the manufacturer's protocol. Quantification was made with an Agilent Bioanalyzer High Sensitivity DNA assay (Agilent, High-Sensitivity DNA Kit, Cat# 5067-4626). Subsequently amplified cDNA was enzymatically fragmented, end-repaired, and polyA tagged. Cleanup/size selection was performed on amplified cDNA using SPRIselect magnetic beads (Beckman-Coulter, SPRIselect, Cat# B23317). Next, Illumina sequencing adapters were ligated to the size-selected fragments and cleaned up using SPRIselect magnetic beads. Finally, sample indices were selected and

ACCELERATED ARTICLE PREVIEW

amplified, followed by a double-sided size selection using SPRIselect magnetic beads. Final library quality was assessed using an Agilent Bioanalyzer High Sensitivity DNA assay. Samples were then sequenced on NovaSeq6000 (Illumina, USA) as paired-end mode (read1: 26bp for cell barcodes, read2: 91bp for RNA reads) to achieve a minimum of 20,000 paired-end reads per cell for gene expression.

Alignment, quantification and quality control of scRNA-seq data

Droplet libraries were processed using Cell Ranger 5.0.0 (10x Genomics, USA). Sequencing reads were aligned with STAR (v2.7.2a)[44] using the GRCh38 human reference genome. Count matrices were built from the resulting BAM files using dropEst[46]. Cells that had fewer than 1,000 UMIs or greater than 20,000 UMIs, as well as cells that contained greater than 10% of reads from mitochondrial genes or Hemoglobin genes, were considered low quality and removed from further analysis. Additionally, putative doublets were removed using Scrublet (v0.2.1) for each sample[47].

scRNA-seq computational pipelines and basic analysis

The R package Seurat (v3.2.2) was used for data scaling, transformation, clustering, dimensionality reduction, differential expression analysis and most visualization[48]. Data were scaled and transformed using the SCTransform() function, and linear regression was performed to remove unwanted variation due to cell quality (% mitochondrial reads). For integration, we identified 3,000 shared highly variable genes (HVGs) using SelectIntegrationFeatures() function. Then, we identified 'anchors' between individual datasets based on these genes using the FindIntegrationAnchors() function and inputted these anchors into the IntegrateData() function to create a batch-corrected expression matrix of all cells. Principal component analysis (PCA) and uniform manifold approximation and projection (UMAP) dimension reduction with 30 principal components were performed[49]. A nearest-neighbor graph using the 30 dimensions of the PCA reduction was calculated using FindNeighbors() function, followed by clustering using FindClusters() function.

Cellular identity was determined by finding differentially expressed genes (DEGs) for each cluster using FindMarkers() function with parameter 'test.use=wilcox', and comparing those markers to known cell type-specific genes (**Extended Data Fig. 7a**). We obtained 12 cell clusters, which were further confirmed using Azimuth (**Fig. 2d** and **Extended Data Fig. 7a,c**)[50]. Six major cell types were defined from 12 clusters as follows; $CD4^+$ T cells [CD4T] and Treg were annotated as CD4T; $CD8^+$ T cells [CD8T] and Proliferative T cells [Pro_T]

ACCELERATED ARTICLE PREVIEW

were annotated as CD8T; natural killer cells [NK] were annotated as NK; B cells [B] and Plasmablast were annotated as B; $CD14^+$monocytes and $CD16^+$monocytes were annotated as monocytes [Mono]; conventional dendritic cells [cDC] and plasmacytoid dendritic cells [pDC] were annotated as Dendritic cell [DC]. To clarify immune cell type-specific expression of DOCK2, we produced the density plot using plot_density() function from Nebulosa R package (v1.0.0)[51], and the dot plot using DotPlot() function.

Droplets labeled as innate immune cell clusters ($CD14^+$monocytes, $CD16^+$monocytes, cDC, and pDC) were extracted and reintegrated for further subclustering using the same procedure as described above except using 2,000 shared HVGs. After integration, clustering and cluster annotation (**Extended Data Fig. 7b**) were performed as described above.

DE analysis using scRNA-seq data

Differential gene expression analysis was performed between severe COVID-19 patients and healthy controls in each cell type. Donor pseudo-bulk samples were first created by aggregating gene counts for each cell type within each sample. Genes which expression rate was more than 10% in either COVID-19 patients or healthy controls in each cell type were included in the analysis. Differential gene expression testing was performed using an NB GLM implemented in the Bioconductor package edgeR (v3.32.0)[52].

***DOCK2* co-expression analysis and GO enrichment analysis**

We applied the weighted gene co-expression network analysis (WGCNA) algorithm[28] to evaluate co-expressed genes with *DOCK2* in COVID-19. Pseudo-bulk normalized data of non-classical monocytes in the COVID-19 patients using scran (v1.18.5)[53] was used for WGCNA analysis, and genes were selected if they were expressed in more than 1% of cells in non-classical monocytes of the COVID-19 patients. We calculated the adjacency with a "unsigned network" option and soft threshold power with the adjacency matrix set to 5, created Topological Overlap Matrix by TOMsimilarity, calculated the gene tree by hclust against 1 - TOM with method = "average", and conducted a dynamic tree cut with the following parameters; deepSplit = 4, minClusterSize = 30. We performed GO enrichment analysis of *DOCK2* co-expression gene module using the function enrichGO (pvalueCutoff = 0.01, pAdjustMethod = "BH",' OrgDb = "org.Hs.eg.db", ont = "BP") of Clusterprofiler (v3.14.3)[54].

Single-cell eQTL analysis of the *DOCK2* risk variant

ACCELERATED ARTICLE PREVIEW

We applied pseudo-bulk approach for single-cell eQTL analysis. First, we performed single-cell-level normalization using scran (v1.18.5)[53]. Gene expression per cell type per sample was then calculated as the mean of log2-transformed counts-per-cell-normalized expression across cells. For principal component (PC) analysis, genes were adopted if they were expressed (UMI count >0) in more than 1% of cells in non-classical monocytes.

In the eQTL analysis of the *DOCK2* variant, dosage effects of the risk variant (rs60200309-A) on the gene expression were evaluated using linear regression models with age, sex, disease severity (included only in COVID-19 analysis) and the top 2 PCs of the gene expression as covariates. *R* statistical software (version 4.0.2) was used for the analysis.

IFN-α production assay using primary blood cells

PBMC were isolated from the blood of 3 healthy donors by Lymphoprep density gradient. pDC cells were purified by negative selection using the Plasmacytoid Dendritic Cell Isolation Kit II (Miltenyi Biotec, USA). To evaluation interferon-α production ability, sorted pDC cells were stimulated with 30 μg/ml CpG-A ODN (D35; Gene Design, Japan) or control. Interferon-α was evaluated 12 hr after stimulation using VeriKine-HS Human Interferon Alpha All Subtype TCM ELISA Kit (PBL, USA). Differences of IFNα production between the groups were evaluated using paired *t*-test.

Chemotaxis assay using primary blood cells

PBMC were isolated from the blood of 19 healthy donors by Lymphoprep density gradient. $CD3^+$ T cells were sorted by magnetic activated cell sorting (MACS). $CD3^+$ T cells (1.0×10^5) in 100 μl RPMI + 0.5% BSA medium ± CPYPP (100 μM; Tocris, UK) were placed in the upper chambers of Transwell (5 μm pore size; Coaster, USA). The lower chambers were filled with 400 μl RPMI medium supplemented with CXCL12 (100 ng/ml; R&D Systems, USA) and incubated at 37℃ for 2 hours. The cells that migrated to the lower chambers were collected and analyzed using FACS. The following monoclonal antibodies were used for FACS analysis: anti-human CD3 (UCHT1; BD Biosciences, USA) and CD4 (SK3; BD Biosciences, USA) antibodies. Dead cells were excluded using zombie dyes (BioLegend; USA). Events were acquired with a LSR Fortessa (BD Biosciences, USA) and analyzed with FlowJo software (BD Biosciences, USA). Differences of chemotaxis between CXCL12 groups and CXCL12 + CPYPP group were evaluated using paired *t*-test.

ACCELERATED ARTICLE PREVIEW

DOCK2 knockdown and IFN-α production assay in THP-1 Blue ISG cells

THP1-Blue ISG (InvivoGen) cells were cultured in 10% FBS, 2 mM L-glutamine, 25 mM HEPES. To generate lentivirus vectors, LentiCRISPR v2 expressing gRNA/Cas9[55], Gag-Pol packaging plasmid psPAX2 (Addgene #12260) and pMD2.G (Addgene #12259) were co-transfected to 293T cells using X-treme GENE 9 DNA Transfection Reagent (Roche). The guide RNA for *DOCK2* knock out and potential off-target effects evaluation[56,57] were in **Supplementary Table 11**. Transfected 293T cells were cultured in Dulbecco's modified Eagle medium with 10% FBS and 50 units/ml penicillin/streptomycin. The cultured medium was replaced 12 hr after transfection. The virus containing supernatants were collected after a further 36 hr and filtered through a 0.45-μm pore-size cellulose acetate filter (Sigma-Aldrich). Then, 2×10^6 THP1-Blue ISG cells were cultured in 2 ml polybrene (8 μg/ml, Millipore)/virus-containing medium. After a 24 hr incubation, infected THP1-Blue ISG cells with virus containing medium were collected, centrifuged (400g, 4 min) and cultured in fresh medium. For selection LentiCRISPR vector expressing cells, infected cells were cultured for 4 days in medium supplemented with 1 μg/ml puromycin 2 days after infection. *DOCK2* knock down efficiency was evaluated through quantitative real-time PCR analysis and western blotting (Abcam#ab124848). THP-1 monocytes are differentiated by 72 h incubation with 20 ng/mL phorbol 12-myristate 13-acetate (PMA, Sigma, P8139). IFN-α was evaluated 6 hr after stimulation (3 μg/ml CpG-A ODN [D35, Gene Design] or control ODN [D35, GC]) using VeriKine-HS Human Interferon Alpha All Subtype TCM ELISA Kit (PBL).

Immunohistochemical analysis of lung samples of COVID-19 pneumonia patients

The patient's samples of lung and hilar lymph node were obtained from autopsied cadaver died from COVID-19 pneumonia (Sample 1, 2, 3) and non-COVID-19 pneumonia (Sample 4, 5). For staining control sample, lung and lymph node tissue section were obtained from the surgically resected lung specimens due to lung cancer. Immunohistochemistry for DOCK2 was performed according to standard procedures. Briefly, formalin fixed paraffin embedded tissue sections of 5 mm were deparaffinized. Antigen retrieval was carried out using pressure cooking (in citrate buffer for 3 min). Endogenous peroxidase activity was blocked by incubating sections in 3% hydrogen peroxide for 5 min. After blocking, tissue sections were incubated with the anti-DOCK2 rabbit polyclonal antibody[58] diluted in 1:1000. The EnVision kit from Dako (Glostrup, Denmark) was used to detect the staining.

ACCELERATED ARTICLE PREVIEW

***In vivo* suppression of DOCK2 in Syrian hamster model with SARS-CoV-2 infection**

Virus: SARS-CoV-2 (JPN/Kanagawa/KUH003)[33], was used in experimental animal model of COVID-19. An aliquot of virus was stored at -80°C until use.

Materials: CPYPP, as DOCK2-Rac1 interaction inhibitor[29], was obtained from Tocris Bioscience (Bristol, UK). CPYPP was dissolved in the dimethyl sulfoxide (DMSO).

Animal experiments: All applicable national and institutional guidelines for the care and use of animals were followed. The animal experimentation protocol was approved by the President of Kitasato University through the judgment of the Institutional Animal Care and Use Committee of Kitasato University (approval no. 21-007). Sample sizes were determined based on our experience with SARS-CoV-2 infection models, and the minimum number of animals was used.

DOCK2 inhibition in Syrian hamster model of SARS-CoV-2 infection

We planned and executed the experimental schedule shown in **Extended Data Fig. 10a**. Six-week-old male Syrian hamsters (CLEA Japan, Inc. Tokyo, Japan) were maintained in the biological safety level 3 experimental animal facility of the Department of Veterinary Medicine, Kitasato University. Sixty-three animals were divided four groups: SARS-CoV-2+CPYPP (n = 29); SARS-CoV-2+vehicle (n = 28); mock+CPYPP (n = 3); and mock+vehicle (n = 3). Animals were intranasally inoculated with $10^{5.8}$ $TCID_{50}$ of SARS-CoV-2 or medium only (mock infection) at a volume of 100 µL, respectively. After 5 min (dpi 0) and 24 hr (dpi 1), animals were intraperitoneally injected with CPYPP (8.4 mg/head; 0.2 mL) or DMSO (vehicle; 0.2 mL). All animals were weighed daily. SARS-CoV-2 infected animals were euthanized on dpi 3, 6 and 11 (8 animals per group on dpi 3 and dpi 6, and 6 animals per group on dpi 11), and then nasal swabs and tissues were collected. Lungs were dissected out from thoracic organs after euthanasia, and lung weights were measured at dpi 0, 3, 6 and 11. Differences of body weight and lung weight between SARS-CoV-2+CPYPP group and SARS-CoV-2+vehicle group were evaluated using two-sided Welch's t-test. Animals were euthanized when reaching the humane endpoint or 11 days after inoculation with SARS-CoV-2. The humane endpoint (weight loss of >25%) was based on the previous study[34].

Syrian hamsters infected with CPYPP or vehicle were euthanized on dpi 3, 6, and 11 for pathological examinations (n = 3). Histopathological examination of the lungs of the hamsters inoculated with SARS-CoV-2 with CPYPP or vehicle was conducted by hematoxylin and eosin staining. Pathological severity scores in the infected hamsters were evaluated as described elsewhere[34]. Briefly, lung tissue sections were scored based on the percentage of

ACCELERATED ARTICLE PREVIEW

inflammation area of the maximum cut surface collected from each animal in each group by using the following scoring system: 0, no pathological change; 1, affected area (≤10%); 2, affected area (<50%, >10%); 3, affected area (<90%, ≥50%); 4, (≥90%) an additional point was added when pulmonary edema and/or alveolar hemorrhage was observed. The total score is shown for individual animals. Immunohistochemistry for alveolar macrophage was performed according to standard procedures. Briefly, FFPE lung tissue section of infected Syrian hamster were incubated with the anti-CD68 mouse polyclonal antibody diluted in 1:400 (Abcam#ab125212). The EnVision kit from Dako (Glostrup, Denmark) was used to detect the staining.

Total RNA of nasal swab was extracted using QIAamp Viral RNA Mini kit (Qiagen, USA) according to the manufacturer's instructions. Each organ was homogenized by adding RLT buffer of QIAamp Viral RNA Mini kit using a multi-bead shocker (Yasui Kikai, Japan). After centrifugation of 10% (w/v) tissue homogenate at 10,000 rpm for 10 min, RNA was extracted from the recovered supernatants using the kit described above. The nucleocapsid (N) gene of SARS-CoV-2 was detected using THUNDERBIRD Probe One-step qRT-PCR (TOYOBO, Japan) and Primer/Probe N2 2019-nCoV (TaKaRa, Japan). To quantify SARS-CoV-2 N gene copies, a standard curve was generated using Positive Control RNA Mix 2019-nCoV (TaKaRa, Japan). Lung cytokine expression profile (IFNs, *IL-6*, and chemokines) were evaluated with the modifications of Ferren et al[59]. Briefly, 100 ng of RNA was converted to cDNA with the ReverTra Ace qPCR RT Master Mix (TOYOBO, Japan). qPCR was performed with the THUNDERBIRD Probe qPCR Mix (TOYOBO, Japan). The primers and probes used are listed in **Supplementary Table 12**. The reaction of all samples was performed in duplicates using QuantStudio 1 Real-Time PCR System (Thermo Fisher Scientific, USA), and the target mRNA expression levels were normalized with GAPDH as a reference gene. Relative expression levels (fold changes) of mRNA from infected animals compared to uninfected animals were calculated by $2^{-\Delta\Delta Ct}$ method using QuantStudio Design and Analysis Software (Thermo Fisher Scientific, USA). Differences of viral load and lung cytokine expression profile between the two groups were evaluated using two-sided Wilcoxon rank sum test.

Statistics and Reproducibility

Figures 2m and **2n** are representative images of immunohistochemical analysis of DOCK2 in COVID-19 pneumonia and control without COVID-19 or pneumonia. **Extended Data Fig.9** shows all of the autopsied cadaver or surgical specimen examined in this study. For

ACCELERATED ARTICLE PREVIEW

immunohistochemical analysis, all experiments were performed at least three sections of lung and hilar lymph node in each sample, and the similar results were confirmed.

Data Availability

GWAS summary statistics and processed count matrices with de-identified metadata of bulk RNA-seq are deposited at the National Bioscience Database Center (NBDC) Human Database with the accession code hum0343 without restriction (https://humandbs.biosciencedbc.jp/en/hum0343-latest). Processed count matrices with de-identified metadata and embeddings of scRNA-seq are also deposited in the form of a Seurat object at the NBDC with the accession code hum0197 without restriction (https://humandbs.biosciencedbc.jp/en/hum0197-latest). GWAS genotype data of the COVID-19 cases are available under controlled access at European Genome-Phenome Archive (EGA) with the accession code EGAS00001006284. The GWAS summary statistics of COVID-19 HGI (release 5) is obtained from https://www.covid19hg.org/results/r5/. The reference for cell type annotation of PBMC in scRNA-seq (pbmc_multimodal.h5seurat) is obtained from https://satijalab.org/seurat/articles/multimodal_reference_mapping.html.

Code Availability

We used publicly available software for the analyses. The software used is listed in the Methods section.

ACCELERATED ARTICLE PREVIEW

References

38. Hirata, M. *et al.* Overview of BioBank Japan follow-up data in 32 diseases. *J. Epidemiol.* **27**, S22–S28 (2017).
39. Sakaue, S. *et al.* Dimensionality reduction reveals fine-scale structure in the Japanese population with consequences for polygenic risk prediction. *Nat. Commun.* **11**, 1569 (2020).
40. Yamamoto, K. *et al.* Genetic and phenotypic landscape of the mitochondrial genome in the Japanese population. *Commun. Biol.* **3**, 104 (2020).
41. Yip, S. P. Sequence variation at the human ABO locus. *Ann. Hum. Genet.* **66**, 1–27 (2002).
42. Ogawa, K. *et al.* A Transethnic Mendelian Randomization Study Identifies Causality of Obesity on Risk of Psoriasis. *J. Invest. Dermatol.* **139**, 1397–1400 (2019).
43. Bolger, A. M., Lohse, M. & Usadel, B. Trimmomatic: A flexible trimmer for Illumina sequence data. *Bioinformatics* **30**, 2114–2120 (2014).
44. Dobin, A. *et al.* STAR: Ultrafast universal RNA-seq aligner. *Bioinformatics* **29**, 15–21 (2013).
45. Li, B. & Dewey, C. N. RSEM: accurate transcript quantification from RNA-Seq data with or without a reference genome. *BMC Bioinformatics* **12**, 323 (2011).
46. Petukhov, V. *et al.* dropEst: pipeline for accurate estimation of molecular counts in droplet-based single-cell RNA-seq experiments. *Genome Biol.* **19**, 78 (2018).
47. Wolock, S. L., Lopez, R. & Klein, A. M. Scrublet: Computational Identification of Cell Doublets in Single-Cell Transcriptomic Data. *Cell Syst.* **8**, 281-291.e9 (2019).
48. Stuart, T. *et al.* Comprehensive Integration of Single-Cell Data. *Cell* **177**, 1888-1902.e21 (2019).
49. McInnes, L., Healy, J. & Melville, J. UMAP: Uniform manifold approximation and projection for dimension reduction. *arXiv* (2018).
50. Hao, Y. *et al.* Integrated analysis of multimodal single-cell data. *Cell* **184**, 3573-3587.e29 (2021).
51. Alquicira-Hernandez, J. & Powell, J. E. Nebulosa recovers single-cell gene expression signals by kernel density estimation. *Bioinformatics* **37**, 2485–2487 (2021).
52. Robinson, M. D., McCarthy, D. J. & Smyth, G. K. edgeR: A Bioconductor package for differential expression analysis of digital gene expression data. *Bioinformatics* **26**, 139–140 (2009).

ACCELERATED ARTICLE PREVIEW

53. Lun, A. T. L., Bach, K. & Marioni, J. C. Pooling across cells to normalize single-cell RNA sequencing data with many zero counts. *Genome Biol.* **17**, 1–14 (2016).
54. Yu, G., Wang, L. G., Han, Y. & He, Q. Y. ClusterProfiler: An R package for comparing biological themes among gene clusters. *Omi. A J. Integr. Biol.* **16**, 284–287 (2012).
55. Sanjana, N. E., Shalem, O. & Zhang, F. Improved vectors and genome-wide libraries for CRISPR screening. *Nat. Methods* **11**, 783–784 (2014).
56. Doench, J. G. *et al.* Optimized sgRNA design to maximize activity and minimize off-target effects of CRISPR-Cas9. *Nat. Biotechnol.* **34**, 184–191 (2016).
57. Concordet, J. P. & Haeussler, M. CRISPOR: Intuitive guide selection for CRISPR/Cas9 genome editing experiments and screens. *Nucleic Acids Res.* **46**, W242–W245 (2018).
58. Nishihara, H. *et al.* Non-adherent cell-specific expression of DOCK2, a member of the human CDM-family proteins. *Biochim. Biophys. Acta - Mol. Cell Res.* **1452**, 179–187 (1999).
59. Ferren, M. *et al.* Hamster organotypic modeling of SARS-CoV-2 lung and brainstem infection. *Nat. Commun.* **12**, 1–17 (2021).

ACCELERATED ARTICLE PREVIEW

Table 1. Association of the *DOCK2* variant with COVID-19 risk in the Japanese population

rsID Chr:position cytoband Allele Gene	Stage (case collection periods)	Age	Phenotype	No. subjects		Risk allele freq. (A)		OR (95%CI)	*P*
				Cases	Controls	Cases	Controls		
rs60200309 5:169519612 5q35 G/A *DOCK2*	GWAS (April 2020 – Jan 2021)	All age	COVID-19 vs control	2,393	3,289	0.12	0.10	1.24 (1.09-1.41)	0.0011
			Severe COVID-19 vs control	990	3,289	0.13	0.10	1.39 (1.16-1.66)	3.1×10^{-4}
		Age < 65	COVID-19 vs control	1,484	2,377	0.12	0.10	1.32 (1.13-1.55)	5.1×10^{-4}
			Severe COVID-19 vs control	440	2,377	0.16	0.10	2.01 (1.58-2.55)	1.2×10^{-8}
	Replication (Feb 2021 – Sep 2021)	All age	Severe COVID-19 vs control	1,243	3,769	0.11	0.11	1.00 (0.85-1.19)	0.96
		Age < 65		833	1,242	0.12	0.10	1.28 (1.02-1.61)	0.033

Uncorrected *P* values are shown.

ACCELERATED ARTICLE PREVIEW

Extended Data legends

Extended Data Fig. 1. Japan COVID-19 Task Force

Japan COVID-19 Task Force is a nation-wide consortium to overcome COVID-19 pandemic in Japan, which was established in early 2020. Japan COVID-19 Task Force consists of >100 hospitals (red dots) led by core academic institutes (blue labels), and collected DNA, RNA, and plasma from the COVID-19 cases along with detailed clinical information. The figure was originally created using sf and ggplot2 R packages based on Global Map Japan version 2.1 Vector data (Geospatial Information Authority of Japan).

Extended Data Fig. 2. A principal component analysis plot of the GWAS participants and manhattan and quantile-quantile plots of the GWAS

(**a, b**) A principal component analysis (PCA) plot of the GWAS participants (COVID-19 cases and controls) along with and without International HapMap populations (**a** and **b**, respectively). (**c**) Manhattan plots and quantile-quantile plots of the Japanese GWAS of COVID-19. Uncorrected *P* values from GWAS analysis are shown. Dotted lines represent the genome-wide significance threshold of $P < 5.0 \times 10^{-8}$.

Extended Data Fig. 3. Regional association plots of the HLA imputation analysis

Regional association plots of the HLA imputation analysis results. Dots represent SNPs and HLA variants with colors according to the legend. Uncorrected *P* values from HLA imputation analysis are shown. Dotted lines represent the genome-wide significance threshold of $P < 5.0 \times 10^{-8}$. HLA genes with the most significant associations in each of the case-control phenotypes are indicated.

Extended Data Fig. 4. ABO blood type associations with COVID-19 in Japanese and cross-population Mendelian randomization analysis of the COVID-19 GWAS

(**a**) Odds ratios of the ABO blood types in the Japanese population are indicated. Dots represent the odds ratios and bars represent the 95 % confidence intervals. *P* values are uncorrected. Detailed results are presented in **Supplementary table 5**. (**b**) Forest plots of the Mendelian randomization (MR) analysis results of causal inference on the COVID-19 GWAS in Japanese (left panel) and Europeans (right panel). Since effect sizes (= beta) of MR are not scalable among phenotypes and populations, normalized beta is indicated. For

ACCELERATED ARTICLE PREVIEW

each phenotype and population, the standard error for the COVID-19 GWAS with the largest sample size (i.e., “COVID-19 vs control” for Japanese and “Self-reported COVID-19 vs control (C2)” for Europeans) was set to be 0.1. Dots represent the effect size normalized beta estimates and bars represent the 95 % confidence intervals. *P* values are uncorrected. The abbreviations of the exposure phenotypes and the detailed MR results are given in **Supplementary Table 6** and **Supplementary Table 7**. BMI; body mass index, T2D; type 2 diabetes, CPD; cigarettes per day, CAD; cardiovascular disease, SBP; systolic blood pressure, DBP; diastolic blood pressure, eGFR; estimated glomerular filtration rate, UA; serum uric acids, RA; rheumatoid arthritis, SLE; systemic lupus erythematosus.

Extended Data Fig. 5. Effect size comparisons of the COVID-19 risk loci between the discovery GWAS and the replication study

Co-plots of the odds ratios and 95% confidence intervals between the discovery GWAS cohort and replication cohort. To focus on the differences in the cases collected in different pandemic waves (initial waves for GWAS and latter waves for the replication), same controls as GWAS were currently used for the cases in the replication. A regression coefficient was estimated based on logarithm of odds ratios. Dots represent the odds ratios and bars represent the 95 % confidence intervals.

Extended Data Fig. 6. Colocalization analysis of the GWAS and eQTL signals at the *DOCK2* locus

Regional colocalization plots of the GWAS signals (severe and younger COVID-19 cases vs controls) and the eQTL signals on *DOCK2* expression in the COVID-19 patients at the *DOCK2* locus. CLPP; colocalization posterior probability. The eQTL effects of the variants around *DOCK2* region are given in **Supplementary Table 10**.

Extended Data Fig. 7. Cell type definition and gene ontology enrichment analysis of *DOCK2* co-expression gene module in the PBMC single cell analysis

(**a**) Violin plots showing the expression distribution of selected canonical cell markers in the 12 clusters of PBMC. The rows represent selected marker genes and the columns represent clusters with the same color as in **Fig. 2d**. (**b**) Violin plots showing the expression distribution of selected canonical cell markers in the 5 clusters of innate immune cell clusters, shown in the same color as in **Fig. 2h**. (**c**) Tile plot showing percentage concordance between the

ACCELERATED ARTICLE PREVIEW

manually annotated 12 clusters and Azimuth annotation. (**d**) The top 25 enriched biological processes by gene ontology (GO) analysis of *DOCK2* co-expression gene module identified by weighted gene co-expression network analysis (WGCNA) in the non-classical monocytes of COVID-19 patients, where *DOCK2* showed the highest cell type-specific expression profile. The color of the dots represents the adjusted *P* values.

Extended Data Fig. 8. Biological impacts of *DOCK2* downregulation in primary cells and *DOCK2* knockdown and Interferon-α production assay in THP-1 Blue ISG cells

(**a**) The impact of *DOCK2* downregulation on interferon-α (*IFN-α*) production ability in pDC. Sorted pDC were stimulated with CpG and/or CPYPP. Data shows means ± s.e.m. (*n* = 3 per group). Differences of *IFN-α* production ability between the groups were evaluated using two-sided paired *t*-test. (**b**) The impact of *DOCK2* downregulation on chemotaxis in $CD3^+$ T cells. $CD3^+$ T cells were stimulated with CXCL12 or CXCL12 + CPYPP (*n* = 19 per group). Differences of chemotaxis between the groups were evaluated using two-sided paired *t*-test. (**c, d**) Knockdown of *DOCK2* by CRISPR system was confirmed by western blotting (**c**) and qRT-PCR. (**d**) Semi-quantitative staining density measure was determined using ImageJ (NIH). Data shows means ± s.e.m. (*n* = 3 per group). Data are compared to control group. *P* values were determined with One-way ANOVA followed by Dunnett's post hoc test. (**e, f**) Activity ratio of SEAP reporter to no treatment group. Reporter was activated by 50 ng/ml LPS (**e**) or 50 μg/ml polyIC (**f**). Data shows means ± s.e.m. (*n* = 3 per group). Data are compared to control group. *P* values were determined with One-way ANOVA followed by Dunnett's post hoc test.

Extended Data Fig. 9. Immunohistochemical analysis for DOCK2

Lung and hilar lymph nodes were obtained from autopsied cadaver (Sample 1-3, 6, 7) or surgical specimen (Sample 4, 5), and stained by anti-DOCK2 polyclonal antibody. Sample 1-3; COVID-19 pneumonia. Sample 4-5; control. Sample 6; non-COVID-19 severe pneumonia. Sample 7; non-COVID-19 mild pneumonia.

Extended Data Fig. 10. *In vivo* suppression of DOCK2 in a Syrian hamster model with SARS-CoV-2 infection

(**a**) Schematic timeline of the experimental procedure. (**b**) Changes in weight of uninfected animals. The error bars represent standard error of the mean. (**c**) Changes in weight of each

ACCELERATED ARTICLE PREVIEW

of the infected animals, corresponding to **Fig 3a**. Three CPYPP-administrated animals reaching humane endpoint were euthanized at dpi 7 and 9, lowering survival rate to 77% (=10/13), while survival of vehicle-administrated animals was 100% (=12/12). The animals were administered with CPYPP (red), or vehicle (blue). (**d**) Histopathological examination of the lungs of infected hamsters. Syrian hamsters were inoculated with SARS-CoV-2 with CPYPP or Vehicle. Syrian hamsters infected with CPYPP or Vehicle were euthanized on dpi 3, 6, and 11 for pathological examinations (n = 3). Shown are pathological findings in the lungs of hamsters infected with the virus on dpi 3, 6, and 11 (hematoxylin and eosin staining). Middle and Right show enlarged views of the area circled in black in Left. (Scale bars, 2.5 mm [Left], 1.0 mm [Middle], and 0.25 mm [Right].) (**e**) Immunohistochemistry for alveolar macrophages. Shown are immunohistochemical findings in the lungs of hamsters infected with the virus on dpi 6 (n = 3 per group). Lung tissue was stained with the anti-CD68 mouse monoclonal antibody. (Scale bars, 0.25 mm.) (**f**) Pathological severity scores in infected hamsters. To evaluate comprehensive histological changes, lung tissue sections were scored based on (**d**) pathological changes. Scores were determined based on the percentage of inflammation area of the maximum cut surface collected from each animal in each group by using the following scoring system: 0, no pathological change; 1, affected area (≤10%); 2, affected area (<50%, >10%); 3, affected area (<90%, ≥50%); 4, (≥90%) an additional point was added when pulmonary edema and/or alveolar hemorrhage was observed. The total score is shown for individual animals. Blue dot and red dot indicate +Vehicle and +CPYPP, respectively.

ACCELERATED ARTICLE PREVIEW

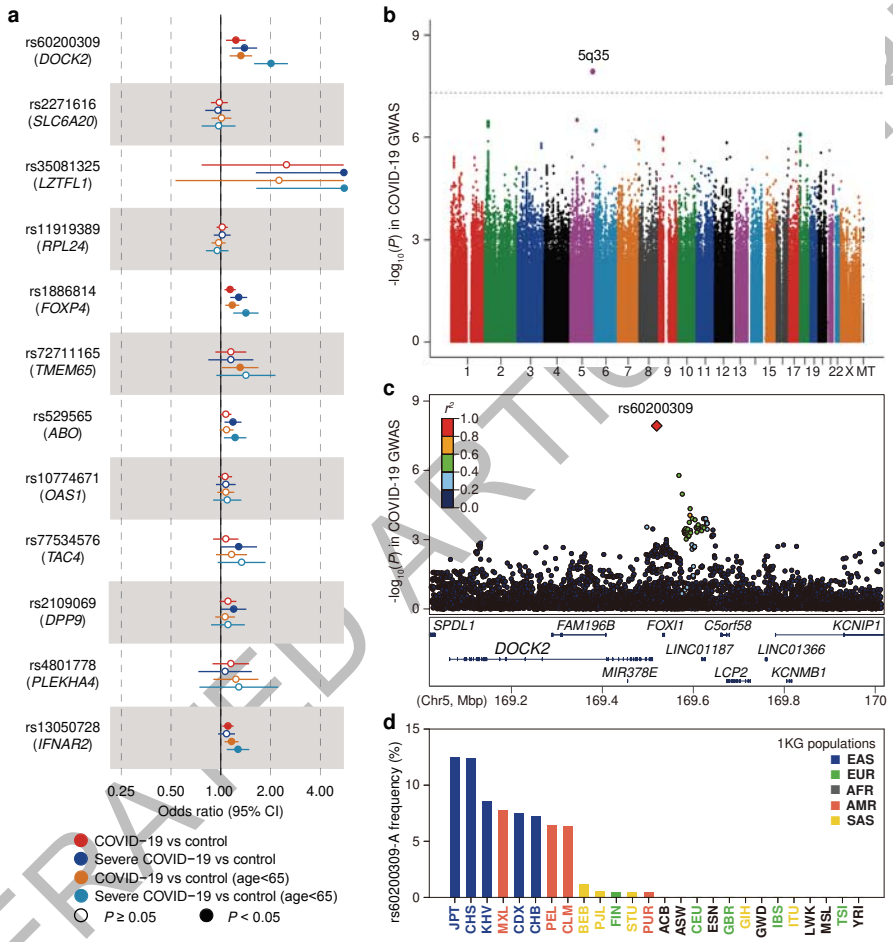

ACCELERATED ARTICLE PREVIEW

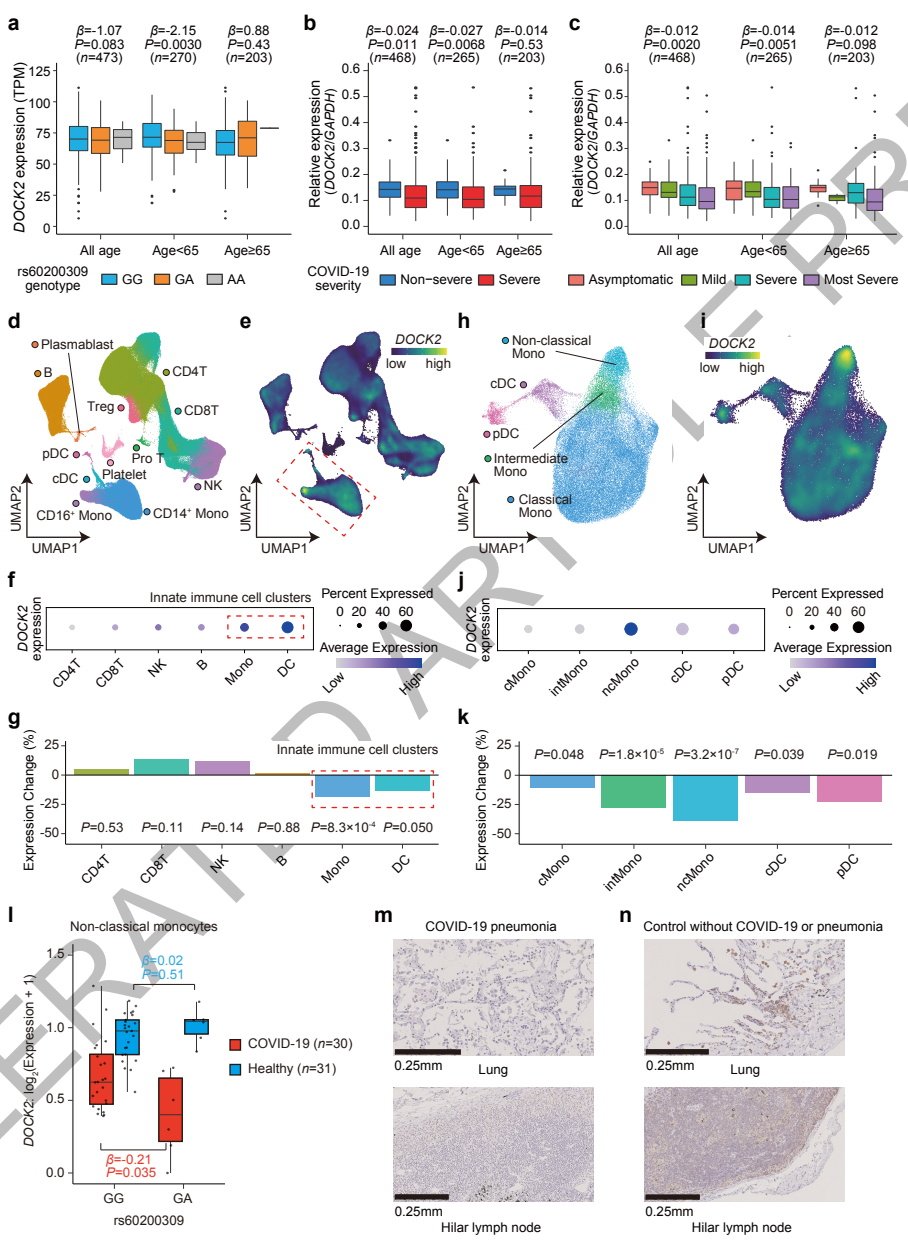
a
β=-1.07
P=0.083
(n=473)
β=-2.15
P=0.0030
(n=270)
β=0.88
P=0.43
(n=203)
DOCK2 expression (TPM)
All age
Age<65
Age≥65
rs60200309 genotype
GG
GA
AA
b
β=-0.024
P=0.011
(n=468)
β=-0.027
P=0.0068
(n=265)
β=-0.014
P=0.53
(n=203)
Relative expression (DOCK2/GAPDH)
COVID-19 severity
Non−severe
Severe
c
β=-0.012
P=0.0020
(n=468)
β=-0.014
P=0.0051
(n=265)
β=-0.012
P=0.098
(n=203)
Asymptomatic
Mild
Severe
Most Severe
d
Plasmablast
B
CD4T
Treg
CD8T
pDC
Pro T
Platelet
cDC
NK
CD16+ Mono
CD14+ Mono
UMAP2
UMAP1
e
DOCK2
low
high
h
Non-classical Mono
cDC
pDC
Intermediate Mono
Classical Mono
i
f
Innate immune cell clusters
Percent Expressed
Average Expression
Low
High
CD4T
CD8T
NK
B
Mono
DC
j
cMono
intMono
ncMono
cDC
pDC
g
Expression Change (%)
P=0.53
P=0.11
P=0.14
P=0.88
P=8.3×10-4
P=0.050
k
P=0.048
P=1.8×10-5
P=3.2×10-7
P=0.039
P=0.019
l
Non-classical monocytes
β=0.02
P=0.51
β=-0.21
P=0.035
COVID-19 (n=30)
Healthy (n=31)
DOCK2: log2(Expression + 1)
rs60200309
m
COVID-19 pneumonia
0.25mm
Lung
Hilar lymph node
n
Control without COVID-19 or pneumonia

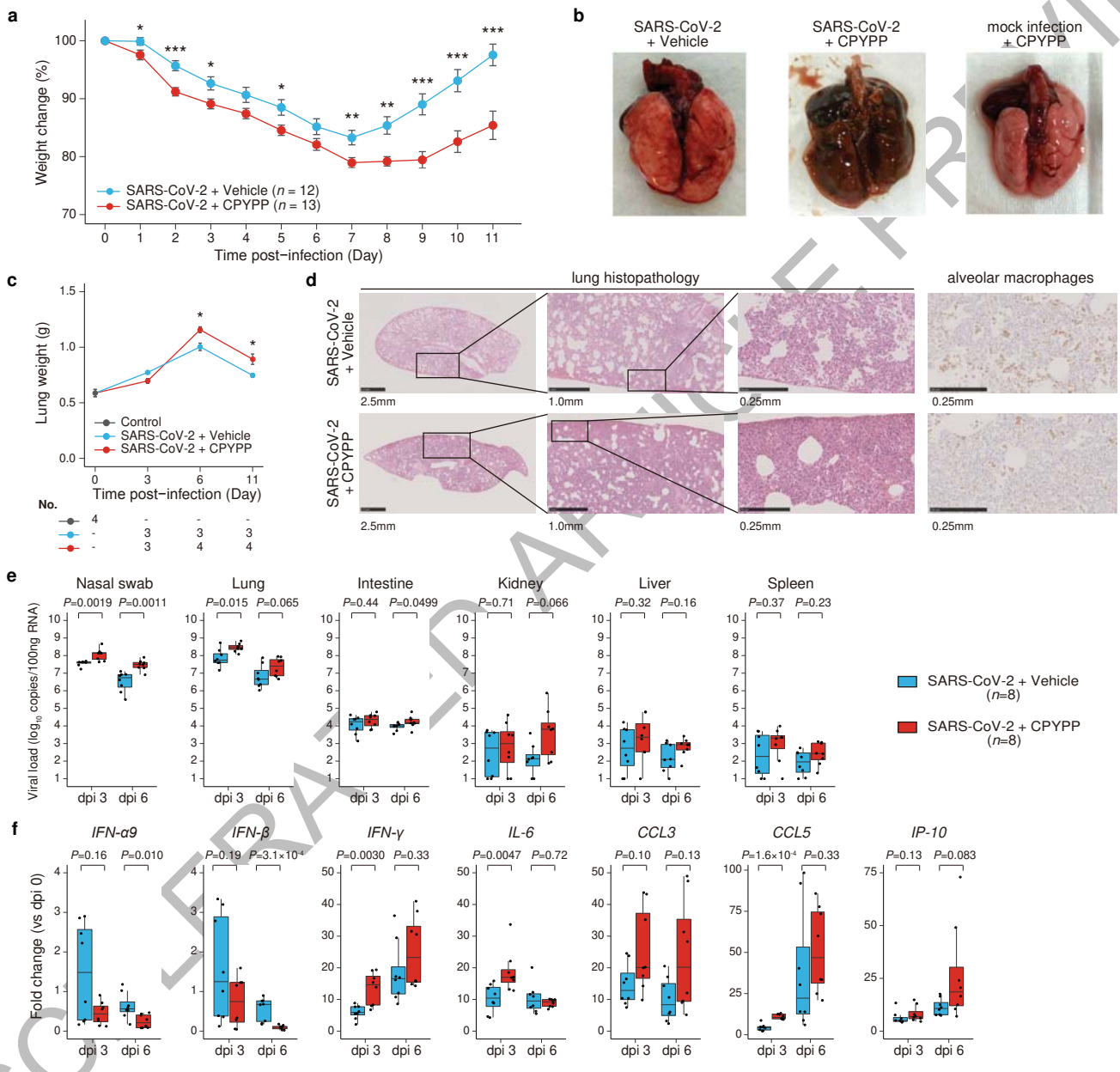

ACCEPTED ARTICLE PREVIEW

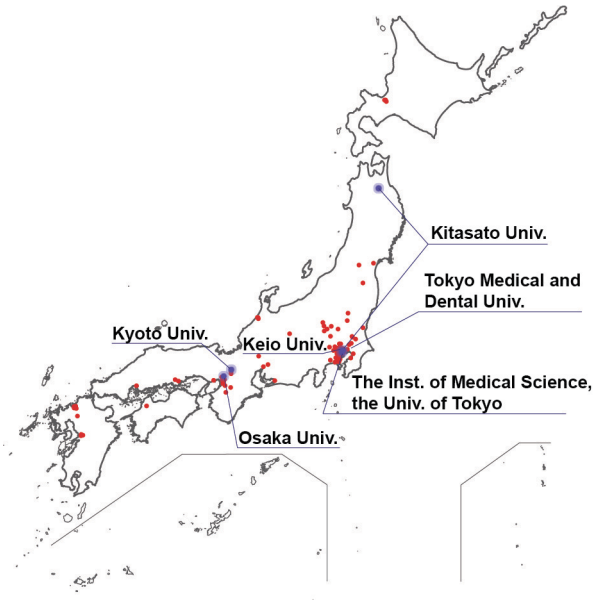

Extended Data Figure 1

ACCELERATED ARTICLE PREVIEW

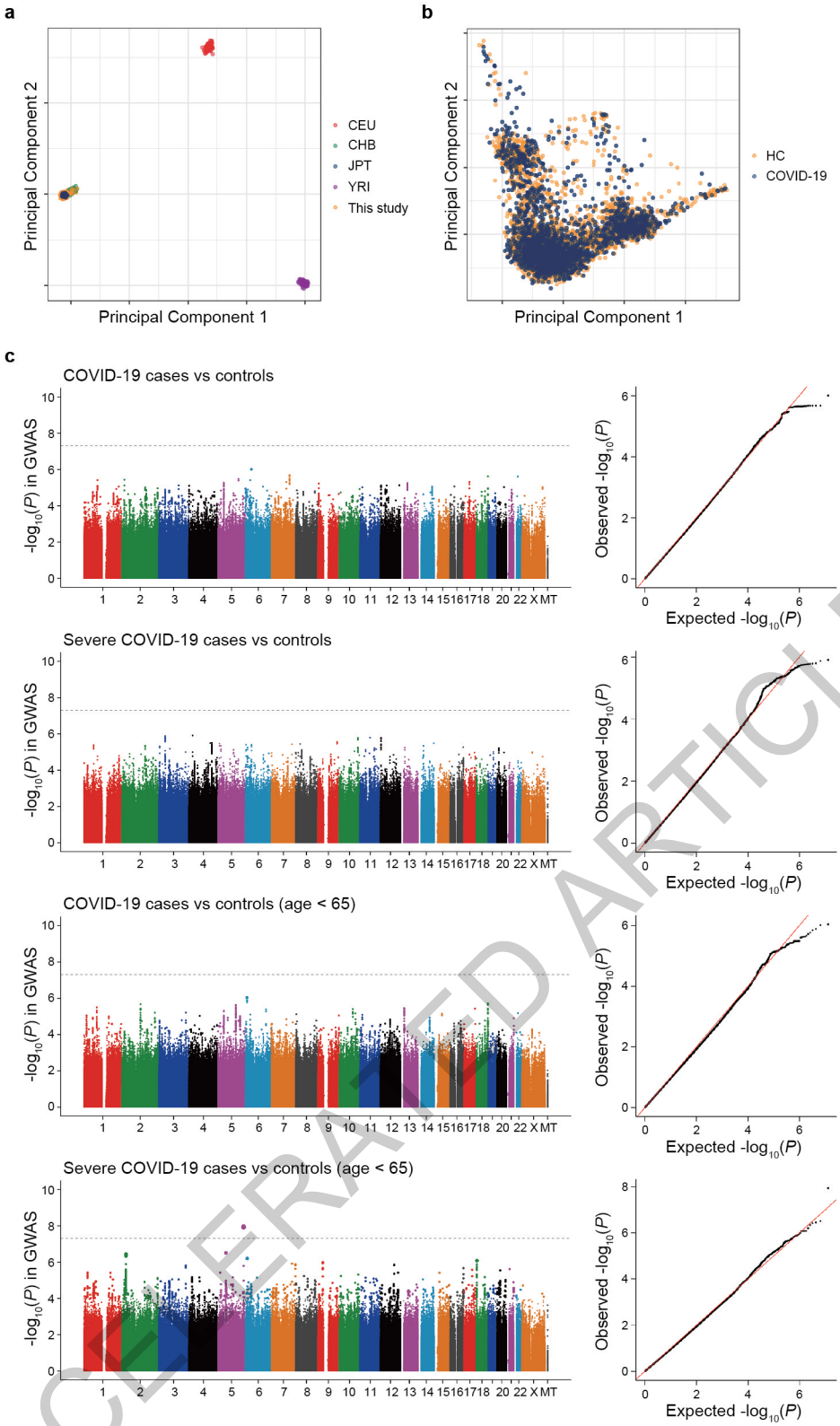

Extended Data Figure 2

ACCELERATED ARTICLE PREVIEW

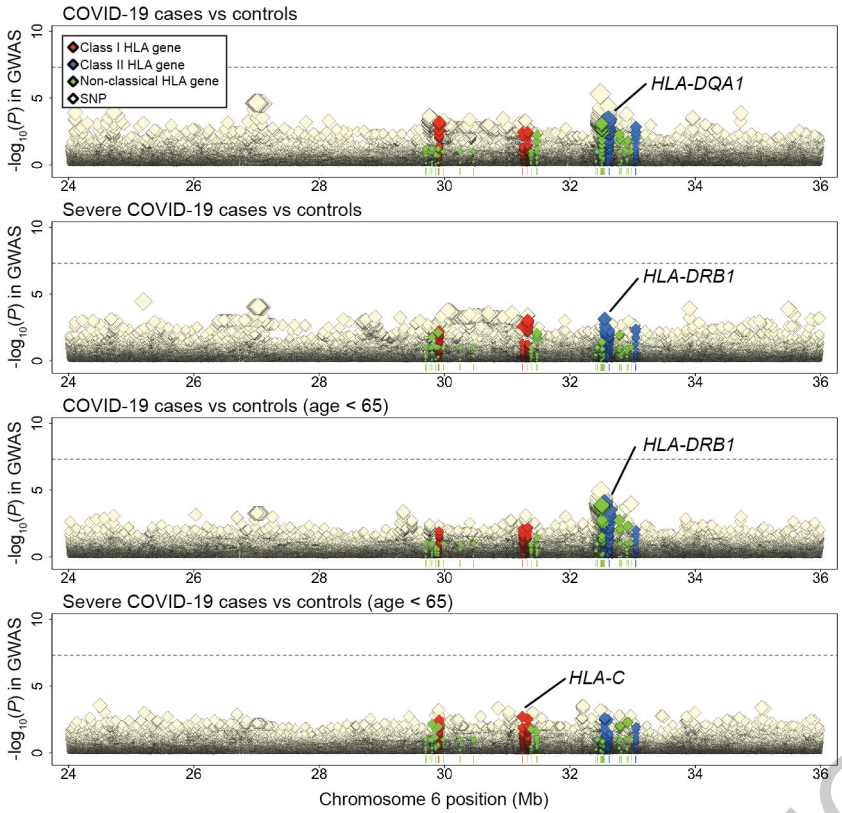

Extended Data Figure 3

ACCELERATED ARTICLE PREVIEW

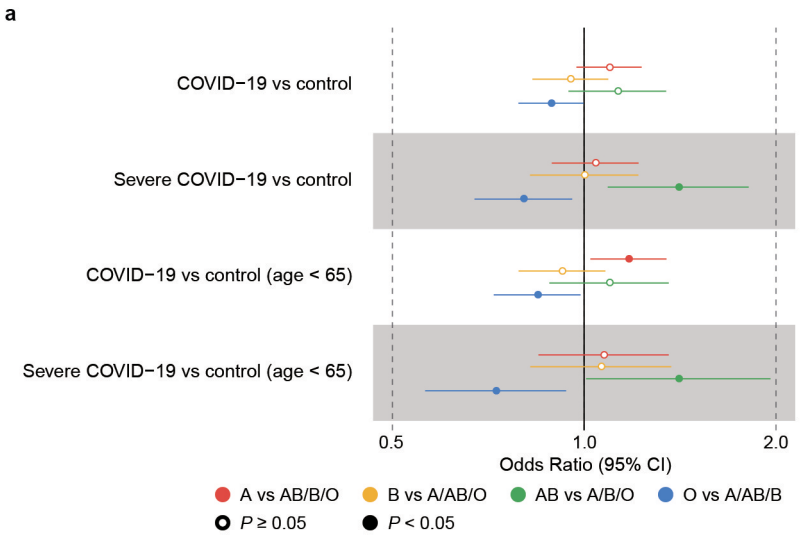

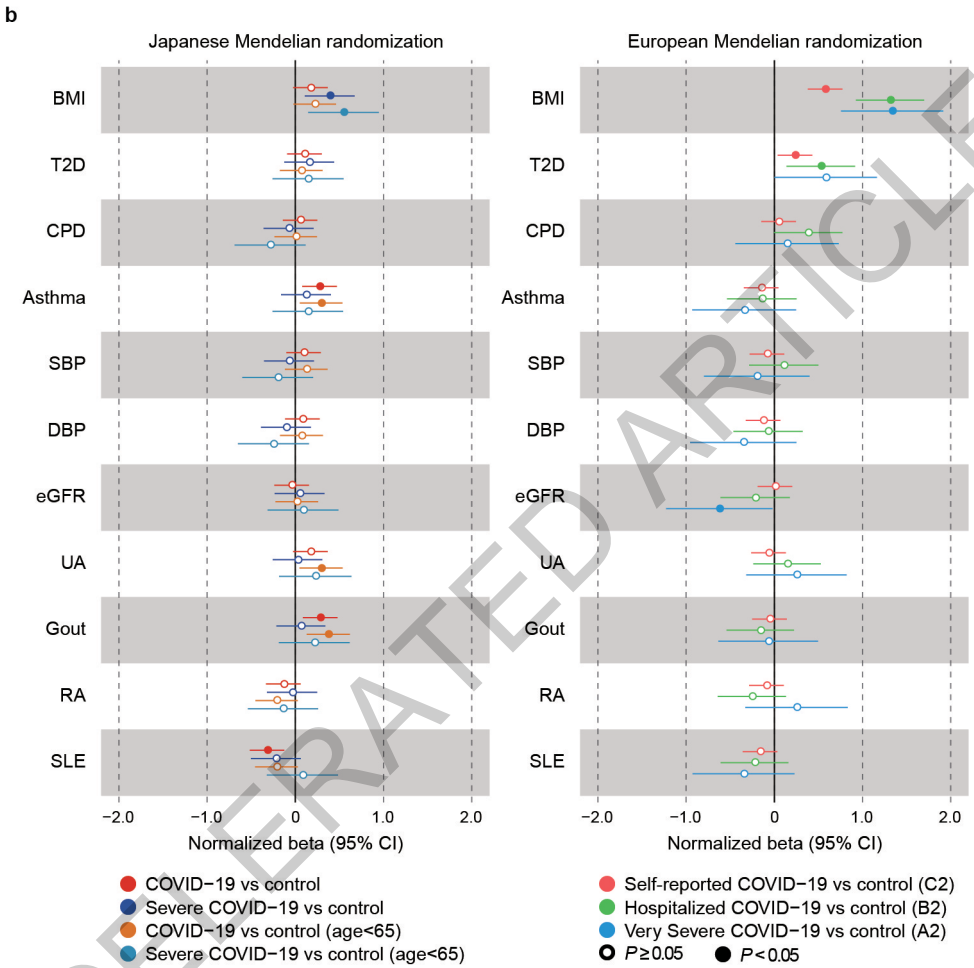

Extended Data Figure 4

ACCELERATED ARTICLE PREVIEW

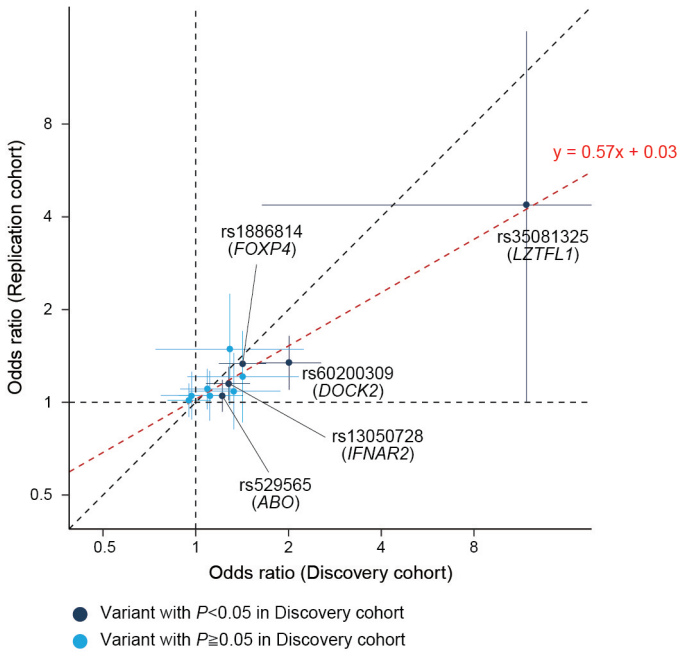

Extended Data Figure 5

ACCELERATED ARTICLE PREVIEW

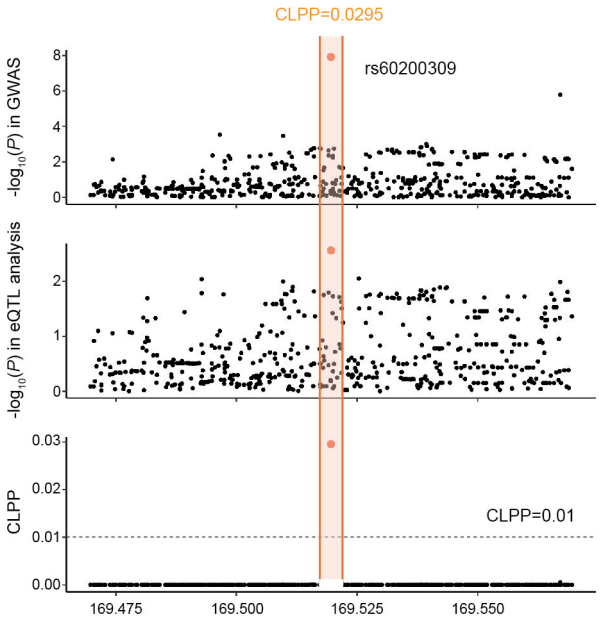

Extended Data Figure 6

ACCELERATED ARTICLE PREVIEW

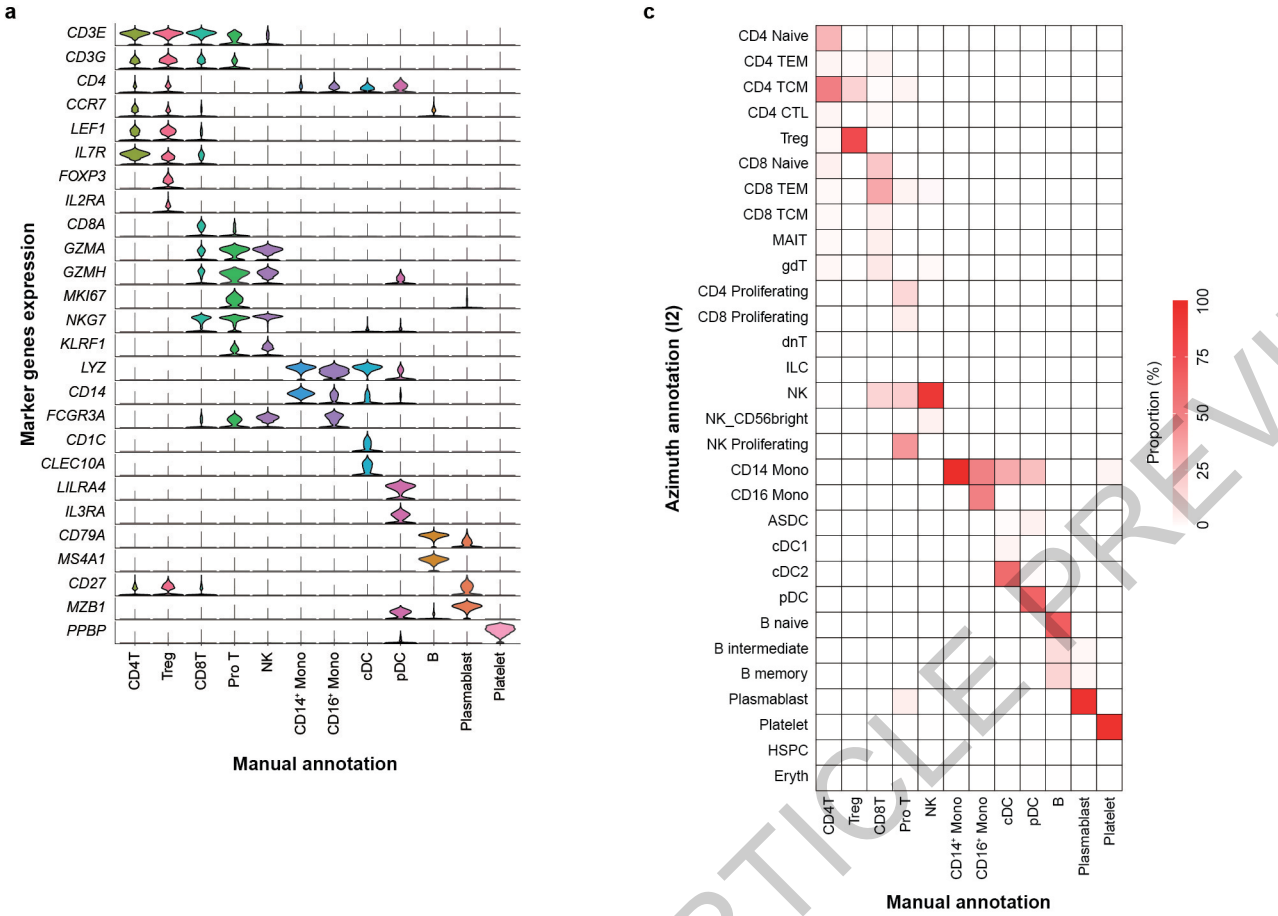

Extended Data Figure 7

ACCELERATED ARTICLE PREVIEW

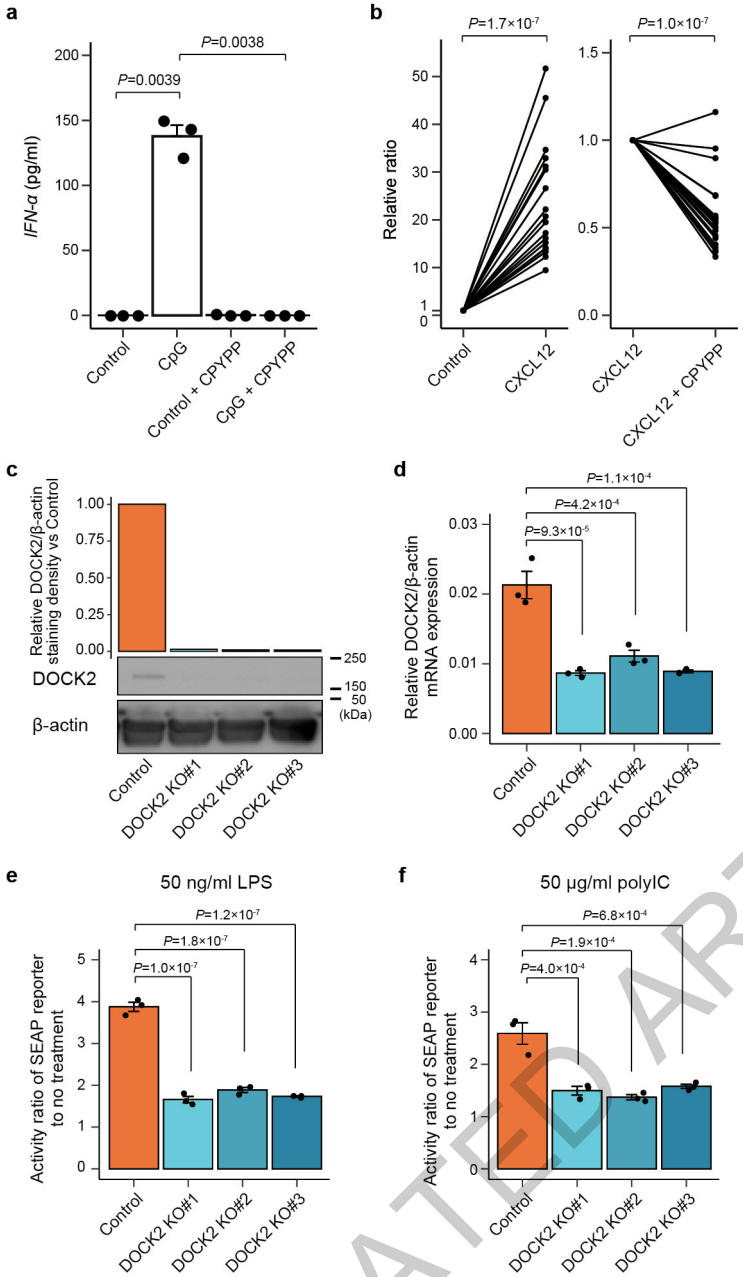

Extended Data Figure 8

ACCELERATED ARTICLE PREVIEW

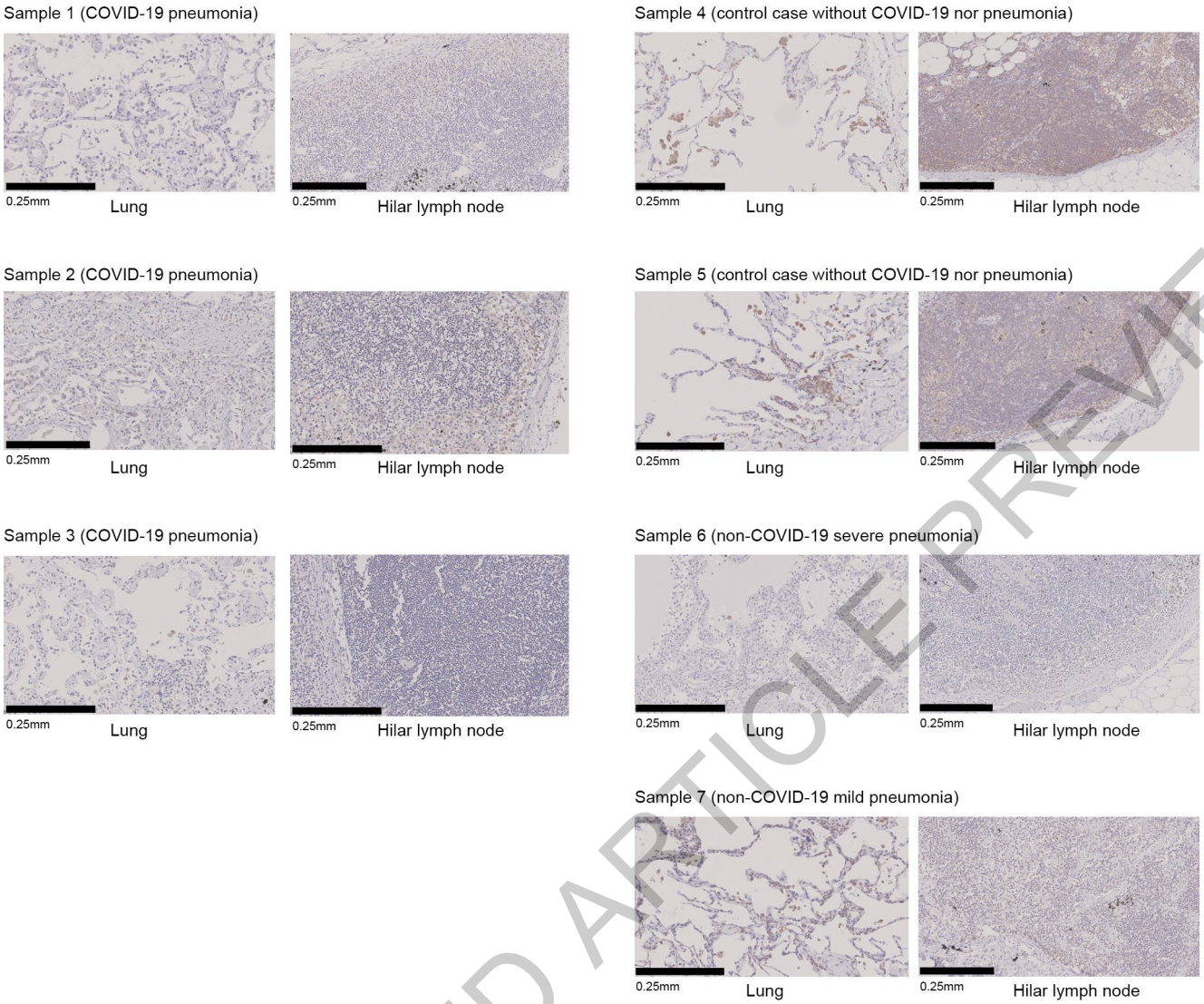

Extended Data Figure 9

ACCELERATED ARTICLE PREVIEW

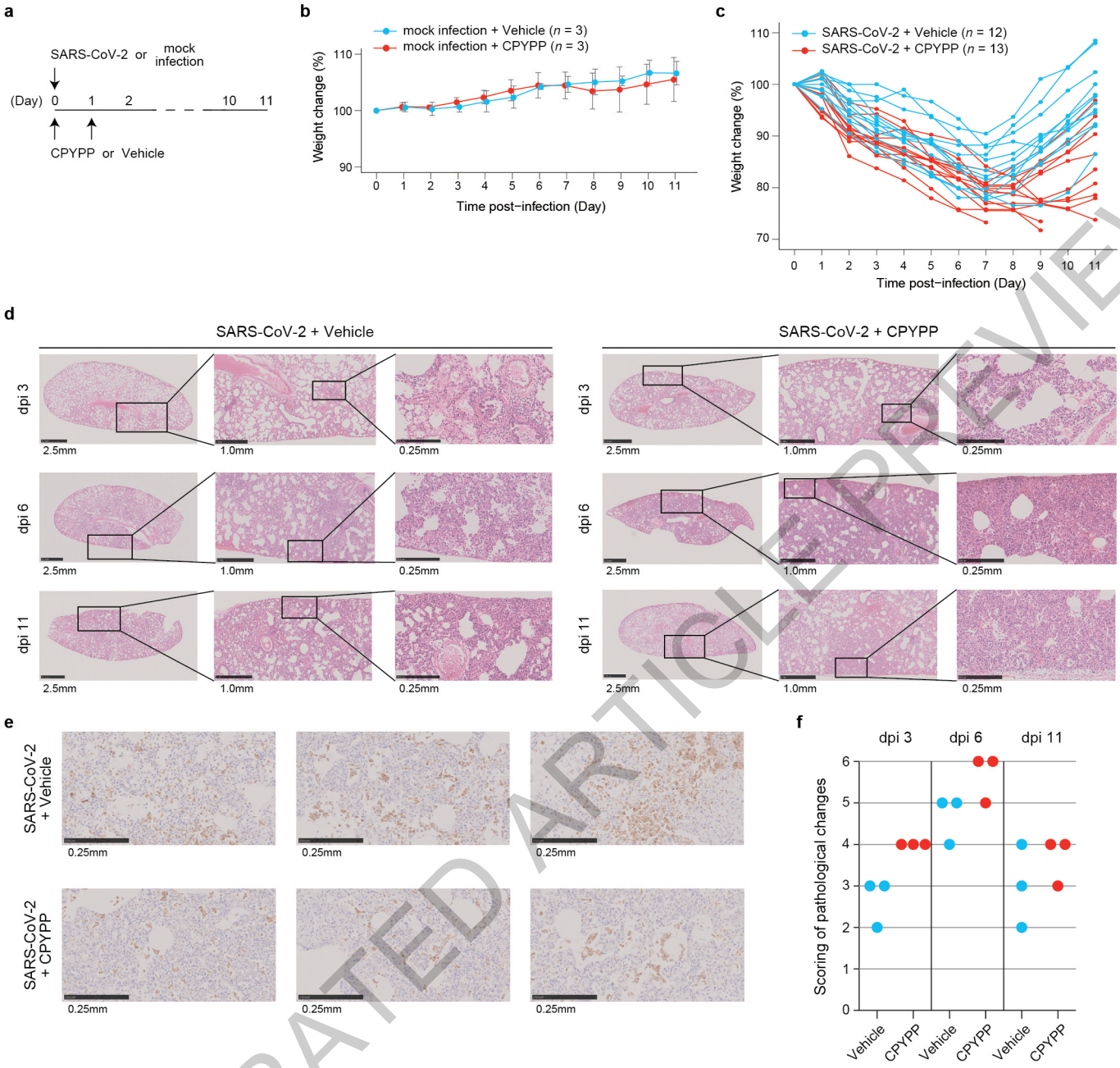

Extended Data Figure 10

ACCELERATED ARTICLE PREVIEW

nature portfolio

Corresponding author(s): Yukinori Okada, Koichi Fukunaga

Last updated by author(s): Jul 28, 2022

Reporting Summary

Nature Portfolio wishes to improve the reproducibility of the work that we publish. This form provides structure for consistency and transparency in reporting. For further information on Nature Portfolio policies, see our Editorial Policies and the Editorial Policy Checklist.

Statistics

For all statistical analyses, confirm that the following items are present in the figure legend, table legend, main text, or Methods section.

n/a	Confirmed
☐	☒ The exact sample size (*n*) for each experimental group/condition, given as a discrete number and unit of measurement
☐	☒ A statement on whether measurements were taken from distinct samples or whether the same sample was measured repeatedly
☐	☒ The statistical test(s) used AND whether they are one- or two-sided *Only common tests should be described solely by name; describe more complex techniques in the Methods section.*
☐	☒ A description of all covariates tested
☐	☒ A description of any assumptions or corrections, such as tests of normality and adjustment for multiple comparisons
☐	☒ A full description of the statistical parameters including central tendency (e.g. means) or other basic estimates (e.g. regression coefficient) AND variation (e.g. standard deviation) or associated estimates of uncertainty (e.g. confidence intervals)
☐	☒ For null hypothesis testing, the test statistic (e.g. *F*, *t*, *r*) with confidence intervals, effect sizes, degrees of freedom and *P* value noted *Give P values as exact values whenever suitable.*
☒	☐ For Bayesian analysis, information on the choice of priors and Markov chain Monte Carlo settings
☒	☐ For hierarchical and complex designs, identification of the appropriate level for tests and full reporting of outcomes
☐	☒ Estimates of effect sizes (e.g. Cohen's *d*, Pearson's *r*), indicating how they were calculated

Our web collection on statistics for biologists contains articles on many of the points above.

Software and code

Policy information about availability of computer code

Data collection	No software was used in data collection.
Data analysis	We used publicly available software for the data analysis (plink 1.9 and 2.0, SHAPEIT2 and 4, Minimac4, DEEP*HLA, TwoSampleMR (v.0.5.5), Trimmomatic (v0.39), STAR (v2.7.9a), RSEM (v1.3.3), eCAVIAR, Cell Ranger 5.0.0, dropEst (v0.8.6), Seurat (v3.2.2 and v4.0.2), Scrublet (v0.2.1), Nebulosa (v.1.0.0), edgeR (v3.32.0), WGCNA (v1.69), scran (v1.18.5), Clusterprofiler (v3.14.3), R (3.6.3 and 4.0.2)).

For manuscripts utilizing custom algorithms or software that are central to the research but not yet described in published literature, software must be made available to editors and reviewers. We strongly encourage code deposition in a community repository (e.g. GitHub). See the Nature Portfolio guidelines for submitting code & software for further information.

Data

Policy information about availability of data

All manuscripts must include a data availability statement. This statement should provide the following information, where applicable:

- Accession codes, unique identifiers, or web links for publicly available datasets
- A description of any restrictions on data availability
- For clinical datasets or third party data, please ensure that the statement adheres to our policy

GWAS summary statistics and processed count matrices of bulk RNA-seq are deposited at the National Bioscience Database Center (NBDC) Human Database with the accession code hum0343 without restriction (https://humandbs.biosciencedbc.jp/en/hum0343-latest). Raw sequencing data of scRNA-seq are available under controlled access at the Japanese Genotype-phenotype Archive (JGA) with accession codes JGAS000543/JGAD000662 for general research use (https://ddbj.nig.ac.jp/resource/jga-study/JGAS000543), which can be accessed through application at the NBDC with the accession code hum0197 (https://humandbs.biosciencedbc.jp/en/hum0197-latest). GWAS genotype data of the COVID-19 cases are available under controlled access at European Genome-Phenome

Archive (EGA) with the accession code EGAS00001006284 for general research use (https://ega-archive.org/studies/EGAS00001006284). GWAS genotype data of the controls collected at Osaka University and the affiliated medical institutes (n=2,380) are available under controlled access at EGA with the accession code EGAS00001006423 for the use as the controls (https://ega-archive.org/studies/EGAS00001006423). GWAS genotype data of the controls collected at University of Tsukuba (n=909) cannot be deposited since no consent was obtained for deposition in a public repository, but these data are available upon request (contact: Prof. Nobuyuki Hizawa; nhizawa@md.tsukuba.ac.jp) for the use as controls in research of inflammatory lung diseases.

Field-specific reporting

Please select the one below that is the best fit for your research. If you are not sure, read the appropriate sections before making your selection.

☒ Life sciences ☐ Behavioural & social sciences ☐ Ecological, evolutionary & environmental sciences

For a reference copy of the document with all sections, see nature.com/documents/nr-reporting-summary-flat.pdf

Life sciences study design

All studies must disclose on these points even when the disclosure is negative.

Sample size	We recruited 2,520 COVID-19 cases who required hospitalization from April 2020 to January 2021 (the 1st to 3rd pandemic waves in Japan) from >100 hospitals participating in Japan COVID-19 Task Force. 3,341 control subjects were collected as general Japanese populations at Osaka University and affiliated institutes. All sample size in GWASs in this study is summarized in Table 1, Supplementary Table2 and 8. Among COVID-19 cases, we enrolled 475 cases for bulk RNA-seq analysis and qPCR-based DE analysis. All sample size in bulk RNA-seq analysis in this study is summarized in Supplementary Table2. We recruited 30 severe COVID-19 cases and 31 healthy controls for PBMC scRNA-seq analysis. We recruited 19 healthy controls for evaluation of biological impacts of DOCK2 downregulation using primary cells. We obtained the samples of lung and hilar lymph node from autopsied cadaver died from COVID-19 pneumonia (N=3), non-COVID-19 pneumonia (N=2) and lung and lymph node tissue section surgically resected due to lung cancer for control sample (N=2).
Data exclusions	We excluded samples with low genotyping call rate, samples in close genetic relation, and ancestry outliers of East Asian population in GWAS analysis. We excluded PCA outliers of gene expression in bulk RNA-seq analysis.
Replication	We enrolled 1,243 severe COVID-19 cases collected from February 2021 to September 2021 (the 4th to 5th pandemic waves in Japan) through Japan COVID-19 Task Force and 3,769 controls as general Japanese populations at Osaka University Graduate School of Medicine, affiliated institutes and the Biobank Japan Project. We replicated an age-specific nominal risk of the DOCK2 variant (rs60200309) in the younger COVID-19 cases (OR=1.28, 95%CI=1.02-1.61, P=0.033). We also obtained the association of the rs60200309 from the pan-ancestry meta-analysis available at https://rgc-covid19.regeneron.com/. We observed the same directional effect with a marginal association signal (OR=1.73, 95%CI=0.95-3.15, P=0.072).
Randomization	We did not need to use randomization in this study because this is a genotype-phenotype association study. All the samples with available accessibility to genotype and phenotype data were included in the analysis.
Blinding	We did not apply blinding of the samples because this is a genotype-phenotype association study and no intervention was conducted in our study.

Reporting for specific materials, systems and methods

We require information from authors about some types of materials, experimental systems and methods used in many studies. Here, indicate whether each material, system or method listed is relevant to your study. If you are not sure if a list item applies to your research, read the appropriate section before selecting a response.

Materials & experimental systems

n/a	Involved in the study
☐	☒ Antibodies
☐	☒ Eukaryotic cell lines
☒	☐ Palaeontology and archaeology
☐	☒ Animals and other organisms
☐	☒ Human research participants
☒	☐ Clinical data
☒	☐ Dual use research of concern

Methods

n/a	Involved in the study
☒	☐ ChIP-seq
☒	☐ Flow cytometry
☒	☐ MRI-based neuroimaging

Antibodies

Antibodies used	Anti-DOCK2 rabbit polyclonal antibody was originally raised using affinity-purified DOCK2 c-terminus antigen in a previous study (Biochim Biophys Acta. 1999; 1452:179-187). anti-DOCK2; Abcam#ab124838 anti-b-actin; Sigma#A5441 anti-CD68; Abcam#ab12512

Validation	Anti-DOCK2 rabbit polyclonal antibody was validated for IHC and western blotting (Blood .2002;100(12):3968-74., Biochem Biophys Res Commun. 2010 Apr 23;395(1):111-5.). Anti-DOCK2 antibody is validated for WB and IHC (Abcam). Anti-β-actin antibody is validated for WB and IF (Sigma). Anti-CD68 antibody is validated for IHC (Abcam).

Eukaryotic cell lines

Policy information about cell lines

Cell line source(s)	THP1-Blue ISG cells (human THP-1 monocyte cell line by stable integration of an interferon regulatory factor (IRF)-inducible SEAP reporter construct)
Authentication	None, but used for experiments within two months after obtaining from the vendor, Invivogen.
Mycoplasma contamination	No mycoplasma
Commonly misidentified lines (See ICLAC register)	None.

Animals and other organisms

Policy information about studies involving animals; ARRIVE guidelines recommended for reporting animal research

Laboratory animals	Syrian hamsters were purchased from CLEA Japan, Inc. Tokyo, Japan. Six-week-old male Syrian hamsters were maintained in the biological safety level 3 experimental animal facility of the Department of Veterinary Medicine, Kitasato University. Animals were cared for according to the Guidelines for Animal Experiments of Kitasato University and the National Institutes of Health Guide for the Care and Use of Laboratory Animals.
Wild animals	Not used in this study.
Field-collected samples	Not used in this study.
Ethics oversight	The animal experimentation protocol was approved by the President of Kitasato University through the judgment of the Institutional Animal Care and Use Committee of Kitasato University (approval no. 21-007).

Note that full information on the approval of the study protocol must also be provided in the manuscript.

Human research participants

Policy information about studies involving human research participants

Population characteristics	COVID-19 cases in the GWAS are of East Asian ancestry, the mean age was 56, 64% were male, and all of them were tested positive for PCR test results. Controls in the GWAS are of East Asian ancestry, the mean age was 53, 48% were male. Mean age of COVID-19 cases in the bulk RNA-seq analysis was 60, 68% were male. Details of the characteristics of the study participants in the GWAS, bulk RNA-seq analysis and replication analysis are summarized in Supplementary Table2.
Recruitment	We enrolled the hospitalized cases diagnosed as COVID-19 by physicians using the clinical manifestation and PCR test results, who were recruited from April 2020 to January 2021 (the 1st to 3rd pandemic waves in Japan) at any of the >100 the affiliated hospitals participating to Japan COVID-19 Task Force. All control participants in GWAS were recruited at Osaka University or related institutions. We incorporated 475 COVID-19 cases collected at the core medical institutes of Japan COVID-19 Task Force and included in the GWAS for bulk RNA-seq analysis and qPCR-based DE analysis. We enrolled severe COVID-19 cases and healthy controls for PBMC scRNA-seq analysis at Osaka University. We recruited healthy controls for evaluation of biological impacts of DOCK2 downregulation using primary cells at Osaka University. We obtained the samples of lung and hilar lymph node from autopsied cadaver died from COVID-19 pneumonia, non-COVID-19 pneumonia and lung and lymph node tissue section surgically resected due to lung cancer for control sample through Japan COVID-19 Task Force.
Ethics oversight	This study was approved by the ethical committees of Keio University School of Medicine, Osaka University Graduate School of Medicine, and affiliated institutes.

Note that full information on the approval of the study protocol must also be provided in the manuscript.